AD-A220 705

A Survey of Electron Cyclotron Waves in the Magnetosphere and the Diffuse Auroral Electron Precipitation

J. L. ROEDER and H. C. KOONS
Space Sciences Laboratory
Laboratory Operations
The Aerospace Corporation
El Segundo, CA 90245

9 March 1990

Prepared for

DTIC
SELECTE
APR 19 1990
B

This report was submitted by The Aerospace Corporation, El Segundo, CA 90245, under Contract No. F04701-85-C-0086-P00019 with the Space Systems Division, P.O. Box 92960, Los Angeles, CA 90009-2960. It was reviewed and approved for The Aerospace Corporation by H. R. Rugge, Director, Space Sciences Laboratory. Lt Fisher was the project officer for the Mission-Oriented Investigation and Experimentation (MOIE) program.
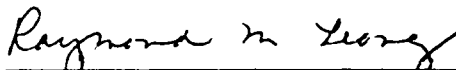
This report has been reviewed by the Public Affairs Office (PAS) and is releasable to the National Technical Information Service (NTIS). At NTIS, it will be available to the general public, including foreign nationals.

This technical report has been reviewed and is approved for publication. Publication of this report does not constitute Air Force approval of the report's findings or conclusions. It is published only for the exchange and stimulation of ideas.

TRYON FISHER, LT, USAF
MOIE Project Officer
SSD/CLFPO

RAYMOND M. LEONG, MAJ, USAF
MOIE Program Manager
AFSTC/WCO OL-AB

REPORT DOCUMENTATION PAGE

1a. REPORT SECURITY CLASSIFICATION	1b. RESTRICTIVE MARKINGS
Unclassified	

2a. SECURITY CLASSIFICATION AUTHORITY	3. DISTRIBUTION/AVAILABILITY OF REPORT
2b. DECLASSIFICATION/DOWNGRADING SCHEDULE	Approved for public release; distribution unlimited.

4. PERFORMING ORGANIZATION REPORT NUMBER(S)	5. MONITORING ORGANIZATION REPORT NUMBER(S)
TR-0088(3940-06)-1	SSD-TR-90-12

6a. NAME OF PERFORMING ORGANIZATION	6b. OFFICE SYMBOL (If applicable)	7a. NAME OF MONITORING ORGANIZATION
The Aerospace Corporation Laboratory Operations		Space Systems Division

6c. ADDRESS (City, State, and ZIP Code)	7b. ADDRESS (City, State, and ZIP Code)
El Segundo, CA 90245	Los Angeles Air Force Base Los Angeles, CA 90009-2960

8a. NAME OF FUNDING/SPONSORING ORGANIZATION	8b. OFFICE SYMBOL (If applicable)	9. PROCUREMENT INSTRUMENT IDENTIFICATION NUMBER
		F04701-85-C-0086-P00019

8c. ADDRESS (City, State, and ZIP Code)	10. SOURCE OF FUNDING NUMBERS			
	PROGRAM ELEMENT NO.	PROJECT NO.	TASK NO.	WORK UNIT ACCESSION NO.

11. TITLE (Include Security Classification)
A Survey of Electron Cyclotron Waves in the Magnetosphere and the Diffuse Auroral Electron Precipitation

12. PERSONAL AUTHOR(S)
Roeder, James L., and Koons, Harry C.

13a. TYPE OF REPORT	13b. TIME COVERED FROM _____ TO _____	14. DATE OF REPORT (Year, Month, Day) 1990 March 9	15. PAGE COUNT 49

16. SUPPLEMENTARY NOTATION

17. COSATI CODES			18. SUBJECT TERMS (Continue on reverse if necessary and identify by block number)
FIELD	GROUP	SUB-GROUP	Plasma waves
			Aurora
			Magnetosphere

19. ABSTRACT (Continue on reverse if necessary and identify by block number)

Natural electron cyclotron harmonic emissions in the outer magnetosphere are often cited as the electron scattering mechanism which results in the diffuse auroral precipitation. A survey is presented of the characteristics of these waves using data from both the SCATHA and AMPTE-IRM plasma wave instruments. The emissions were observed most often in the 0300-0600 LT sector at $L \sim 4-8$ and magnetic latitudes in the range $\pm 10°$. In this region, emissions exceeding 35 $\mu V \, m^{-1}$ were detected only 25% of the time and those exceeding 12 $\mu V \, m^{-1}$ were detected 60% of the time. In agreement with Belmont et al. (J. Geophys. Res. 88, 9163, 1983), these amounts are grossly insufficient to account for the diffuse auroral electron precipitation by quasilinear pitch angle diffusion.

20. DISTRIBUTION/AVAILABILITY OF ABSTRACT	21. ABSTRACT SECURITY CLASSIFICATION
☒ UNCLASSIFIED/UNLIMITED ☐ SAME AS RPT. ☐ DTIC USERS	Unclassified

22a. NAME OF RESPONSIBLE INDIVIDUAL	22b. TELEPHONE (Include Area Code)	22c. OFFICE SYMBOL

DD FORM 1473, 84 MAR
83 APR edition may be used until exhausted.
All other editions are obsolete

PREFACE

We wish to express our appreciation to our many colleagues who
participated in the development, testing, integration, and data reduction
for the SCATHA and AMPTE experiments. In particular, we are indebted to
H. Lühr of the Institut für Geophysik und Meteorologie der Technischen
Universität Braunschweig for making available the AMPTE magnetometer
data. We are grateful to L. R. Lyons and J. F. Fennell for many helpful
discussions.

Accession For	
NTIS GRA&I	☑
DTIC TAB	☐
Unannounced	☐
Justification	
By	
Distribution/	
Availability Codes	
Dist	Avail and/or Special
A-1	

CONTENTS

FIGURES

TABLE

I. INTRODUCTION

Narrowband electrostatic wave emissions at frequencies above the local
electron cyclotron frequency have been cited as the cause of the diffuse
auroral electron precipitation [see the reviews by Swift, 1981, Kennel and
Ashour-Abdalla, 1982, and Coroniti, 1985]. These wave emissions are known
variously as electron cyclotron harmonic (ECH) waves or 'n+1/2' waves since
they tend to occur at odd half-multiples of the electron cyclotron
frequency. The role of these waves in forming the diffuse aurora has been
questioned by Belmont et al. [1983], who reported the lack of intense waves
observed by the geostationary spacecraft GEOS 2. Lyons [1984b] suggested
that the strong ECH wave emissions might occur at radial distances beyond
the GEOS orbit. In this report we report the results of a survey of such
wave emissions in the magnetosphere at geocentric radial distances of 4-20
R_e. The conclusions are shown to be similar to that of Belmont et al.
[1983]: the frequency of occurrence and amplitude of the observed emissions
are insufficient to account for the global diffuse auroral pattern.

The diffuse aurora is a broad band (several hundred km) of weak
electron and ion precipitation (0.1-3 erg cm^2 s^{-1}) around the entire
auroral oval. In this report we will be concerned only with the diffuse
electron precipitation. On the evening side of the oval this band is
usually smooth and structureless, while on the morning side it tends to be
patchy and somewhat variable. There may be discrete arcs imbedded in the
diffuse band in both the morning and evening sectors. Visible light images
from the ground and satellites [Lui and Anger, 1973; Lui et al., 1973]
have shown that the diffuse aurora exists almost continuously for all local
times. These data, however, do not provide a quantitative measure of the
particle precipitation spectrum. In-situ measurements of the precipitating
electron flux show one characteristic that sets the diffuse aurora apart
from the discrete arcs. This is the absence in the diffuse aurora of
field-aligned acceleration of particles due to electric fields parallel to

7

the geomagnetic field. Low altitude observations of the precipitating electron flux show a spectrum which decreases monotonically with energy above 1 keV. Representative spectra of the evening sector precipitation have been published by Deehr et al. [1976], Winningham et al. [1978], and Meng et al. [1979]. Observations on the morning side have been reported by Gustafsson [1973] and Lyons and Fennell [1986]. Above a certain energy threshold (approximately 0.2-1 keV) the spectrum is usually well represented by a Maxwellian spectrum. The commonly observed excess flux at energies below this threshold has been attributed to backscattered and secondary particles from the atmosphere [Meng et al., 1979]. The density and temperature of the Maxwellian seem to mirror the typical characteristics of the central plasma sheet.

There have been many studies of the location of the boundaries of the diffuse auroral precipitation [for example Fairfield and Viñas, 1984; Gussenhoven et al., 1983; Horwitz et al., 1986; Newell and Ming, 1987]. These investigations have usually concentrated on the equatorward boundary, which is assumed to be magnetically conjugate with the inner edge of the magnetospheric plasma sheet. Using DMSP electron data, Gussenhoven et al. [1983] found that the corrected geomagnetic latitude of the equatorward boundary was related in an approximately linear way to the value of the K_p index of geomagnetic activity. The boundary was found to be at minimum latitude near 0300 LT, ranging from 67° for $K_p=0$ to 57° for $K_p=5$. The maximum latitude was detected near 1500 LT with values in the range 72-64° for the same range of K_p. Gussenhoven et al. [1983] attempted to map these boundaries along the geomagnetic field to the equatorial plane. It was found that the boundary for $K_p=5$ ranged from a minimum radius L=3.5 at 0300 LT to a maximum of L=9.5 at 1500 LT. When $K_p=0$ the boundary expanded and the minimum and maximum radii rotated in local time to L=7.5 at 0900 LT and L=10.2 at 2100 LT, respectively. Newell and Meng [1987] have recently reported a study of the equatorward boundary of the diffuse aurora as a function of the particle energy. It was found that in some respects the pattern of electron precipitation matches approximately a model pattern of

particle convection boundaries in the equatorial magnetosphere. Studies
such as these serve as a reference to check the boundaries of whatever
process causes the precipitation.

There exist two types of processes which could cause the violation of
the first adiabatic invariant of plasma sheet electrons, resulting in the
precipitation of those electrons. The first mechanism is the scattering of
the electrons by gradients of the magnetospheric magnetic fields with scale
lengths comparable to the electron cyclotron radius [Lyons, 1984a;
Birmingham, 1984]. Because of the small cyclotron radius of electrons of
keV energies, the large field gradients that are needed are found only in
the current sheet of the distant magnetotail. Lyons [1984a] reports that
electron precipitation from this process would have energies of 0.1-100 keV
and be limited to the high-latitude boundary of the auroral oval.
Birmingham [1984] investigated similar phenomena in the Jovian magneto-
sphere. These characteristics contrast sharply with the energy spectrum
and latitudinal extent of the observed electron precipitation. For these
reasons it has been assumed that the precipitation is due to the second
mechanism, which is pitch angle scattering of the electrons by plasma
waves.

An observable which can be related to the intensity of the electron
scattering process is the pitch angle anisotropy of the electron
distribution. The limit of strong diffusion is defined as the level of
wave amplitude which is capable of scattering an electron across the width
of the loss cone in a single bounce period, thus completely isotropizing
the distribution [Kennel, 1969]. The wave intensity required to cause
strong diffusion of particles at a given energy is easily calculated, and
so this limit serves as a benchmark against which all observations are
compared. Because of the small angular width of the loss cone in the
equatorial region of auroral field lines, the level of anisotropy is very
difficult to observe by high altitude instruments. Many researchers have
used data from low altitude satellites to ascertain more easily the
electron pitch angle distribution within and near the loss cone. For

9

example, Sharber [1981] presented evidence in ISIS-2 data that the pitch angle distribution of the electron precipitation is isotropic only in a small region of precipitation near the middle of the diffuse auroral band. Several investigators have compared low-altitude observations of the electron loss cone with near-simultaneous conjugate particle observations in the equatorial plasma sheet. Most of these comparisons between low and high altitude observations use high altitude data at pitch angles well outside the loss cone. Such comparisons are relevant to the diffusion calculation only if the level of scattering is near the strong diffusion limit. Meng et al. [1979], using DMSP and ATS-6 data, concluded that for several cases the precipitation within the loss cone was identical in magnitude and spectral shape to the 60° pitch angle particles at the equator. Recently, Schumaker et al. [1987] reached the same conclusion concerning thirteen out of fourteen possible cases of P78-1 and SCATHA data. These reports of the isotropy of the electron distribution seem to indicate that the electrons were undergoing strong diffusion by some type of wave interaction. In contrast to these results, Fairfield and Viñas [1984] surveyed the particle measurements by the ISEE-1 spacecraft near the equatorial plane and found substantial anisotropy levels at pitch angles near 90°. The calculations of Lyons [1974] indicate that the level of the diffusion rate at large pitch angles due to electrostatic waves is much smaller than the rate near the loss cone. For this reason, the aniso-tropies observed by Fairfield and Viñas [1984] may not be susceptible to smoothing by the waves.

The amplitudes of electrostatic ECH emissions typically observed by the plasma wave experiment on the OGO 5 satellite were very large (approximately 10 mV m^{-1}). Kennel et al. [1970] and Scarf et al. [1973] suggested that these intense waves could be responsible for pitch angle diffusion of electrons of energies 1-10 keV which were observed in the diffuse auroral precipitation. Shaw and Gurnett [1975] reported ECH emissions of 10 mV m^{-1} amplitude that were detected by Imp 6 at radial distances beyond the plasmapause up to 10 R_e. The ISEE spacecraft detected ECH waves

10

with amplitudes as large as 1 mV m^{-1} in this region [Gurnett et al., 1979]. Koons and Fennell [1983] emphasized the transient nature of ECH waves by noting that these emissions were detected by SCATHA only during sporadic, highly time-dependent particle injection events. This characteristic of the wave emissions is in sharp contrast to the continuous and large-scale spatial nature of the diffuse precipitation.

Using quasilinear plasma theory, Lyons [1974] calculated electron diffusion rates corresponding to a 10 mV m^{-1} ECH wave. Lyons [1974] concluded that the waves were sufficiently strong to cause precipitation consistent with the auroral observations. At this point all observations seemed to fit a consistent picture formulated by Ashour-Abdalla and Kennel [1978] and Kennel and Ashour-Abdalla [1982]. The similarity of the precipitation spectrum to its plasma sheet source implied that the precipitation mechanism was not a strong function of the particle energy. Particle diffusion by plasma waves is a likely candidate to fulfill this requirement. The low energy range of the electrons suggested that the causal plasma waves were electrostatic, because of their low resonant energy compared to electromagnetic waves. Isotropy of the electron distribution meant that strong diffusion was at work, and the electrostatic waves of the required magnitude were observed.

This theory was challenged by Belmont et al. [1983], which cited measurements of electrostatic waves by the GEOS-1 and GEOS-2 satellites. Gough et al. [1981] and Canu [1982] presented surveys of the ECH wave power observed in geosynchronous orbit by the GEOS spacecraft. This work indicated that the occurrence frequency of intense ECH emissions was very low and that the distribution of such emissions was much more localized around the geomagnetic equator than was previously assumed by Lyons [1974]. Previously, Fredricks and Scarf [1973] had also reported that most of the intense emissions observed by OGO 5 occurred near the magnetic equator.

The trapping of ECH emissions within regions near the magnetic equator is generally assumed to be due to refraction of the waves by field and

11

density gradients [Barbosa,1980; 1985]. Engel and Kennel [1984; 1985] performed calculations that showed that the refraction of upper hybrid waves by the parallel magnetic field gradient tends to limit the total amplification of the convective instability which generates the waves. The ECH emissions should be susceptible to similar effects, although a study of this has not been published.

Belmont et al. [1983] reported that the wave amplitude of 1 mV m^{-1} was exceeded during only 2% of the time when the GEOS spacecraft was within 3° of the magnetic equator. Very near the equator this amplitude was exceeded only 15% of the time. The diffusion rate computations by Belmont et al. [1983] which were consistent with the GEOS data implied that ECH emissions cannot be the sole cause of the diffuse auroral precipitation. Lyons [1984b] speculated that the waves of the needed amplitude might occur at radial distances larger than the orbits of geosynchronous spacecraft like GEOS. This controversy was also reviewed by Coroniti [1985].

There has been only one direct comparison between the observations of the level of diffuse electron precipitation and the intensity of plasma waves near the equator. For this purpose Fontaine et al. [1986] used low-altitude particle data from the ARCAD-3 satellite and measurements of the particles and fields in the plasma sheet by GEOS-2. These observations show that the electron distribution was isotropic to within a factor of 2-5, and that the wave intensity was too low to support this level of precipitation.

In this report we present a survey of ECH emissions in the outer magnetosphere to help resolve the questions regarding the source of the diffuse electron precipitation. Such a survey has also been suggested by Barbosa [1980] to aid in the investigation of the generation of ECH emissions by plasma instabilities. In the following sections we present several cases of the AMPTE plasma wave data in detail, and review the results of a statistical analysis of both the AMPTE data and the SCATHA data. The characteristics of the observed wave emissions are then compared with the morphology of the diffuse auroral electron precipitation.

II. INSTRUMENTATION

The plasma wave survey makes use of data from the plasma wave experiments on both the SCATHA and the AMPTE Ion Release Module (IRM) spacecraft. The nearly geosynchronous orbit of SCATHA and the highly elliptical path of the AMPTE-IRM have proven to be very complementary for this study.

The SCATHA satellite follows a moderately elliptical orbit (7.8 R_e apogee, 5.3 R_e perigee) with an inclination of 7.8°. The VLF receiver data from the SCATHA spacecraft consist of a wideband channel with two possible frequency ranges: 0-3 kHz and 0-5 kHz, and a set of eight narrowband channels with center frequencies of 0.4, 1.3, 2.3, 3.0, 10.5, 30, 100, and 300 kHz, respectively [Fennell, 1982]. The wideband channel is equipped with an automatic gain control (AGC) circuit, and the fixed-gain narrowband channels each have relative bandwidths of ±7.5%. The experiment employs two antennas to distinguish between electrostatic and electromagnetic emissions. An air-core loop antenna detects the magnetic component of the waves, and a 100-m tip-to-tip dipole detects the electric component. The sensitivity of the electric field receiver is 0.5 μV m^{-1} Hz$^{-1/2}$ at 1.3 kHz. The sensitivity of the magnetic receiver is 3 × 10^{-6} nT Hz-$^{1/2}$ at 1.3 kHz. The dynamic range of both the electric and magnetic data is three orders of magnitude. The receiver can process signals from only one antenna at a time, and is normally switched between the electric and magnetic signals every 16 s.

The AMPTE IRM satellite is in a highly elliptical orbit (18.83 R_e apogee, 557 km perigee, and 28.6° inclination). The plasma wave instrument on board the IRM spacecraft consists of a variety of antennas and signal processors to measure electric and magnetic fields over the range of frequencies from 31 Hz to 5.6 MHz [Häusler et al., 1985]. This report will consider only the data from the Stepped Frequency Receiver (SFR). The SFR has three spectrum analyzers that may be switched to either

the electric or magnetic antennas by command. The analyzers process a complete 32-channel spectrum every second in the frequency ranges 0.2-2.6 kHz, 0.9-9.0 kHz, and 9-99 kHz, respectively. The electric antenna is a 47-m tip-to-tip dipole, and the magnetic antenna is a boom-mounted search coil magnetometer. The sensitivity of the electric measurement on AMPTE is approximately 0.02 μV m^{-1} $Hz^{-1/2}$. The sensitivity of the magnetic data channel is set by the spacecraft noise level, which is approximately 10-5 nT HzD1/2. The dynamic range of both measurements is three orders of magnitude. The magnitude of the DC magnetic field is computed from the data taken by the magnetometer on the IRM. This instrument provides a three-component vector at 32 times every second [Luhr et al., 1985].

III. OBSERVATIONS

In order to introduce the data from the plasma wave instrument on the IRM, we present two passes of the spacecraft through the magnetosphere. These examples will illustrate the extremely tenuous nature of the ECH waves and their apparent trapping at the magnetic equator. Figure 1 shows a spectrogram of one of the strongest examples of ECH emissions observed by the IRM over its two-year life. The figure is partitioned into three panels, each of which displays the electric field data from a 32-channel analyzer. The data have been time averaged with period of 16 s. The bottom panel shows the data in the frequency range 0.2-2.6 kHz, the middle panel shows the data from 0.9 to 9.0 kHz, and the top panel shows the data from 9 to 99 kHz. The linear frequency scales are marked on the left side of the figure. The data are color coded according to the scale on the right side of the figure. The horizontal reddish lines at the bottom of each panel are calibration signals and represent approximately the largest amplitude allowable for each analyzer. The abscissa is marked with the universal time, the spacecraft geocentric distance in earth radii, and the local time in hours. The dark line plotted in the middle and bottom panels represents the value of the electron cyclotron frequency f_{ce}, as computed from the measured magnetic field.

The 4 h of data shown in Figure 1 are from an outbound pass of the IRM through the dawn sector of the magnetosphere on December 6, 1984. This pass provides a good example of the ECH emissions observed by AMPTE between local midnight and dawn. The two intense bands of emissions below f_{ce} in the lower panel can be identified as whistler mode waves. The gap between the two bands occurs at precisely $f_{ce}/2$. Because of the overlapping frequency ranges of the SFR channels, these two bands also appear in the lower left section of the middle panel. Above the dark line marking f_{ce} in the lower and middle panels are the ECH emissions. The instrument detected electric field emissions in the first harmonic band (between f_{ce} and $2f_{ce}$) almost continuously from 0120 UT until 0355 UT. These waves become
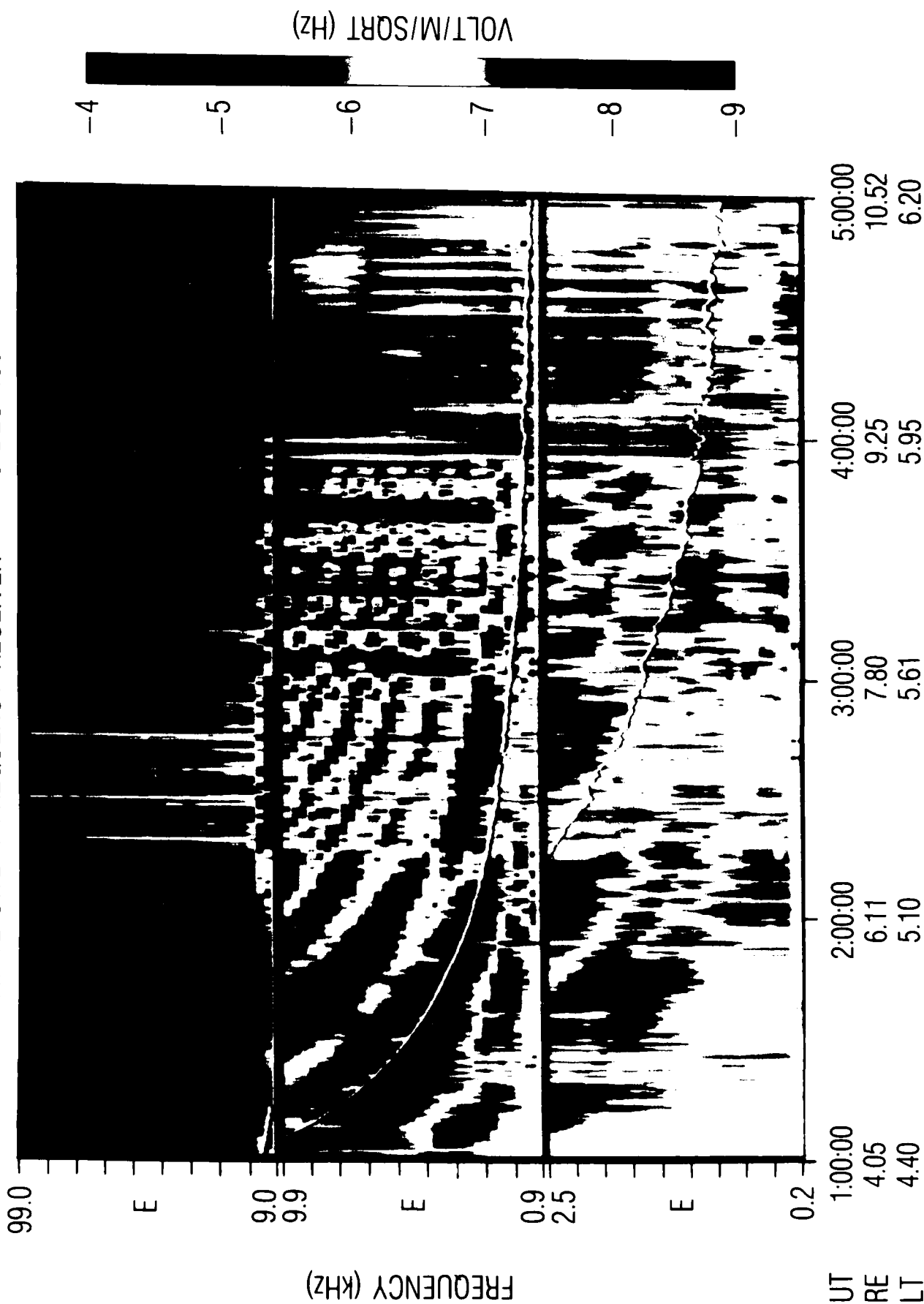
Fig. 1. Spectrogram of 4 h of the electric field spectral density detected by AMPTE in the frequency range 200 Hz - 100 kHz on December 6, 1984.

especially intense from 0223 UT to 0353UT, which caused the analog electronics within the SFR instrument to saturate intermittently. The vertical spikes in the top panel of the spectrogram are artifacts due to this nonlinear saturation by the ECH waves. It is estimated that the ECH emissions during this period reached a peak spectral density above 80 μV m^{-1} $Hz^{-1/2}$. The spectral shape of the emissions is extremely variable, sometimes with multiple peaks within the band. Slightly less intense emissions are also detected in the higher cyclotron harmonic bands. The horizontal line in the top panel at a frequency of 66 kHz was interference from the spacecraft power subsystem. The broadband emissions in the top panel which fall in frequency from 50 kHz to 10 kHz are presumed to be electromagnetic nonthermal continuum radiation.

Figure 2 shows a spectrum of SFR data averaged over 10 s of the intense emissions of Figure 1 when the instrument was not undergoing saturation. Data from the low frequency and high frequency channels are plotted as solid lines, and the data from the mid-frequency channel are shown as a dashed line. The spectra from the different analyzers do not match exactly in the frequency ranges in which they overlap. This discrepancy is due to the time variation of the emissions and the differences in the bandwidth and timing of the analyzers. The arrow near the bottom of the figure marks the average value of f_{ce} during this time interval. There were two distinct emissions in the first harmonic band (from f_{ce} to $2f_{ce}$): a strong line at a frequency of 1.7 f_{ce} and a much weaker emission just above f_{ce}. The stronger of these reached a peak intensity of 38 μV m^{-1} $Hz^{-1/2}$ with a bandwidth of 225 Hz or $\Delta f/f_{ce}$ ~ 15% (full width at half maximum). This spectral density and bandwidth correspond to a total amplitude of 0.6 mV m^{-1}. The emissions in the higher harmonic bands were of comparable amplitude to the fundamental line. The additional field amplitude added by the higher harmonic emissions has, however, been shown to be theoretically unimportant to the electron scattering process [Kennel and Ashour-Abdalla, 1982; Belmont et al., 1983]. In this report we will characterize ECH emissions by the amplitude of the electric field in the first harmonic band only.

WAVE ELECTRIC FIELD SPECTRAL DENSITY
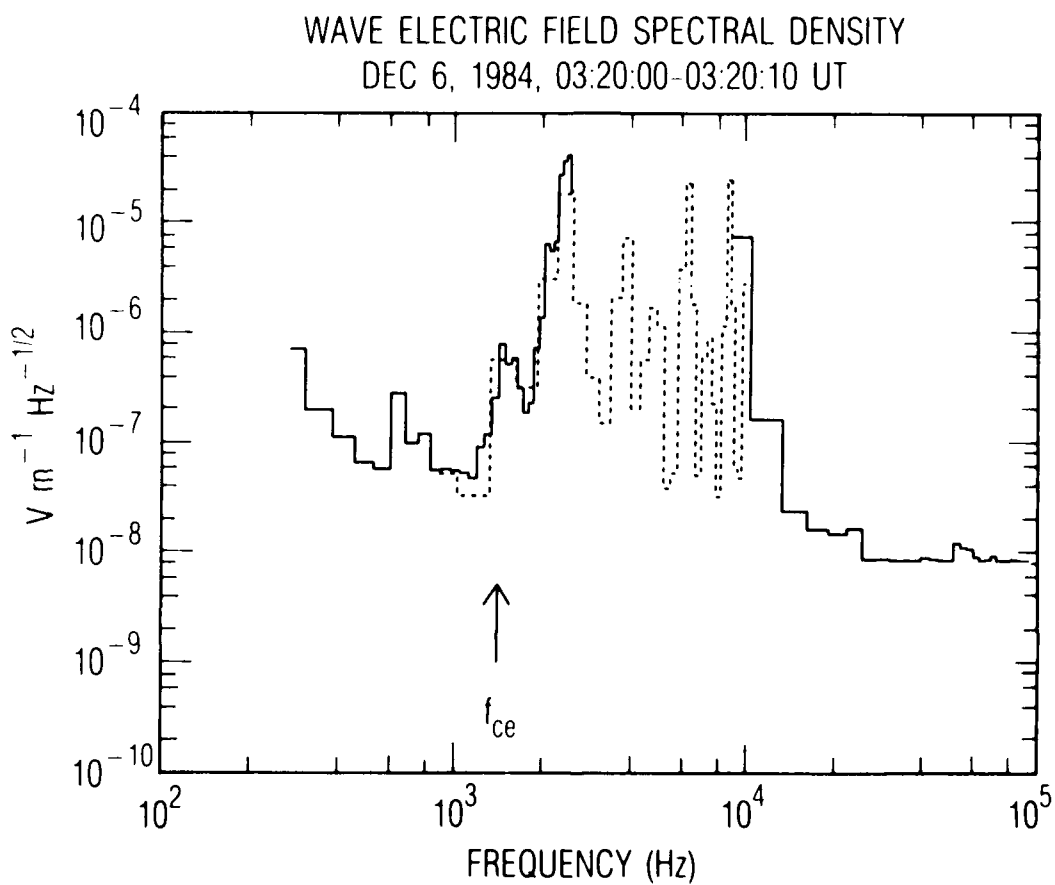### DEC 6, 1984, 03:20:00-03:20:10 UT

Fig. 2. Spectral density as a function of frequency of the electric field averaged over 10 s during the electron cyclotron emissions on December 6, 1984.

The 60-s averages of the total wave electric field amplitude integrated over the band from f_{ce} to $2f_{ce}$ are shown in Figure 3 for the data of December 6. The amplitude was computed from a composite spectrum constructed from the SFR data. The wave field in this band during this period is almost entirely due to ECH emissions which maximize at approximately 0237 UT at a peak amplitude of almost 2 mV m^{-1}. The amplitude may be underestimated during the intervals in which the instrument was saturated, but this occurred less than 5% of the time during this pass. For the last hour of this plot, the ECH emissions become very transient and much weaker (less that 0.1 mV m^{-1}) except for an intense 2-min burst at 0448 UT. The peaks at 0406 UT and 0449UT in Figure 3 are somewhat contaminated by the broadband electric field emissions visible in Figure 1.

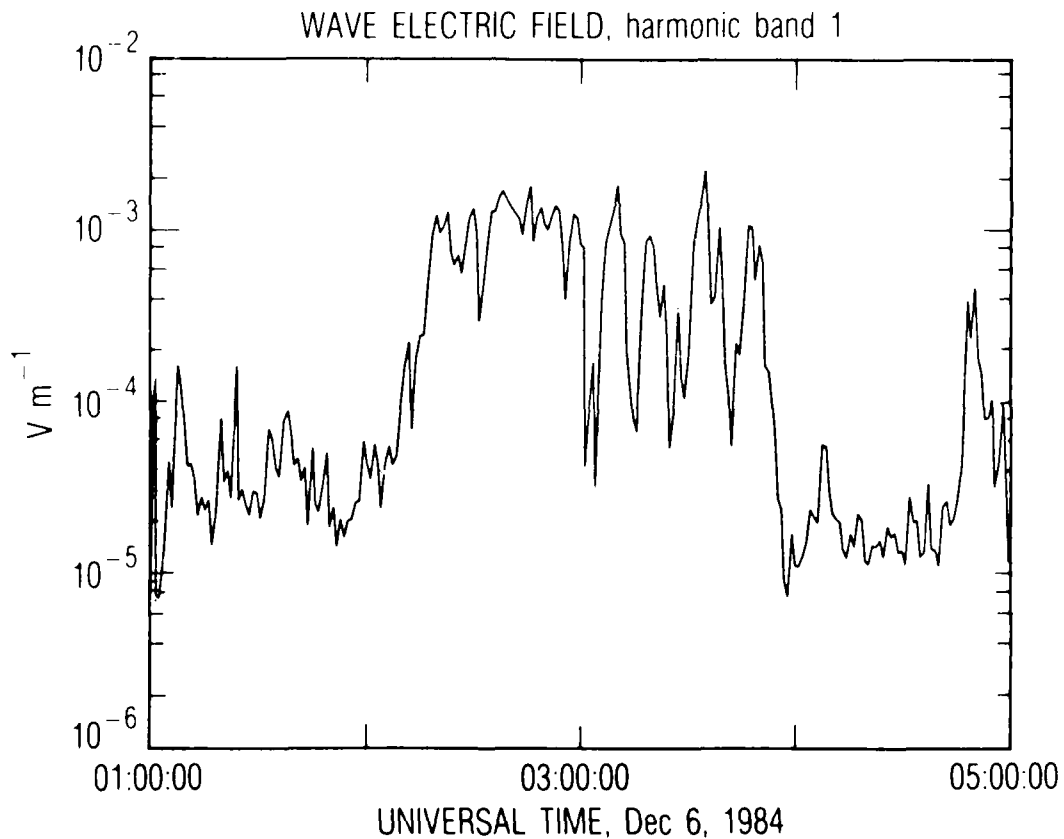WAVE ELECTRIC FIELD, harmonic band 1

UNIVERSAL TIME, Dec 6, 1984

Fig. 3. Electric field amplitude computed from the AMPTE spectral density data of Fig. 1 by integrating over the frequency from the electron cyclotron frequency to its first harmonic. Amplitudes are plotted as 60-s averages.

The magnetic coordinates of the IRM position on December 6 are shown as a function of time in Figure 4. The three panels present the values of the McIlwain radial parameter, the magnetic local time in hours, and the dipole latitude in degrees computed using a magnetic field model. One may note that as the IRM moved out from $L=4.3$ to $L=10.5$, its dipole latitude decreased from $12°$ to $5.5°$. The weakness of the emissions at $L<6.5$ can be ascribed to the equatorial trapping of the waves. The lack of waves for $L>9$ may be due to some other effect, since the spacecraft model latitude remains approximately constant after 0300 UT. However, the accuracy of the geomagnetic field model becomes somewhat tenuous at higher L values where the distortion by the flow of the solar wind is dominant.
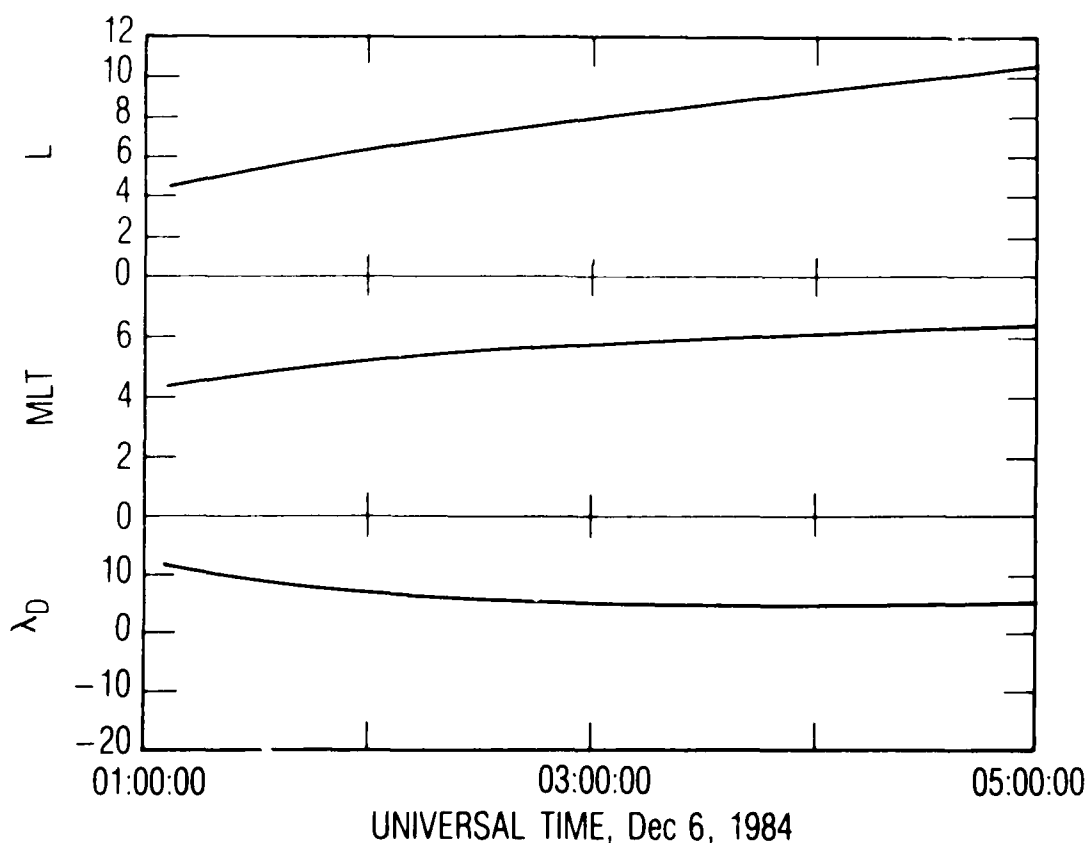

Fig. 4. Magnetic ephemeris of the AMPTE Ion Release Module during the pass of December 6, 1984.

Past local dawn toward noon, the ECH waves tend to become less frequently detected at radial distances below 8 R_e. To illustrate this we present an IRM pass on November 10, 1984, in Figure 5. The format of this spectrogram is the same as that of Figure 1. The entire magnetosphere is profiled from 5.6 R_e to the magnetopause at 10.8 R_e, but the only emissions of more than moderate intensity are found at radii in the range 7.7-9.1 R_e. Examination of the magnetic ephemeris of the IRM on November 10 shows that the satellite did not reach magnetic latitudes below 10° during this pass and that the minimum latitude was achieved at approximately 0745 UT. This may explain the lack of emissions detected by the instrument at other times during this interval.

Figure 6 presents the average spectrum of the electric field during the most intense emission detected on November 10. ECH emissions are clearly observed in the first and third harmonic bands. The fundamental emission at 1.75 f_{ce} has a relative bandwidth of 20% and a total amplitude of 0.25 mV m^{-1}. These two passes have been chosen to represent the strongest waves observed by the IRM in 1.5 years of operation. Fifteen other passes for a variety of locations and conditions were studied in detail using similar techniques. The ECH emissions were generally found to be very weak (less than 10 μV m^{-1}) with a relative bandwidth in the range of 10-20%. The bandwidths of the waves observed by AMPTE are in good agreement with the published values of the typically observed bandwidths of ECH emissions [Kennel and Ashour-Abdalla, 1982].

For the statistical study of the ECH emissions, 1.5 years of data from the IRM were examined to determine the times at which the satellite crossed the magnetopause. This determination was performed by noting the character of the observed wave emissions and by using the survey plots of the data from the plasma instrument and magnetometer. Approximately 500 spectrograms were identified in which the spacecraft was inside the magnetosphere. Each spectrogram consisted of 4-s averages of the SFR data for a 1-h interval. Each spectrogram was split into six 10-min intervals for the survey. Each interval was examined, and several quantities were entered

23
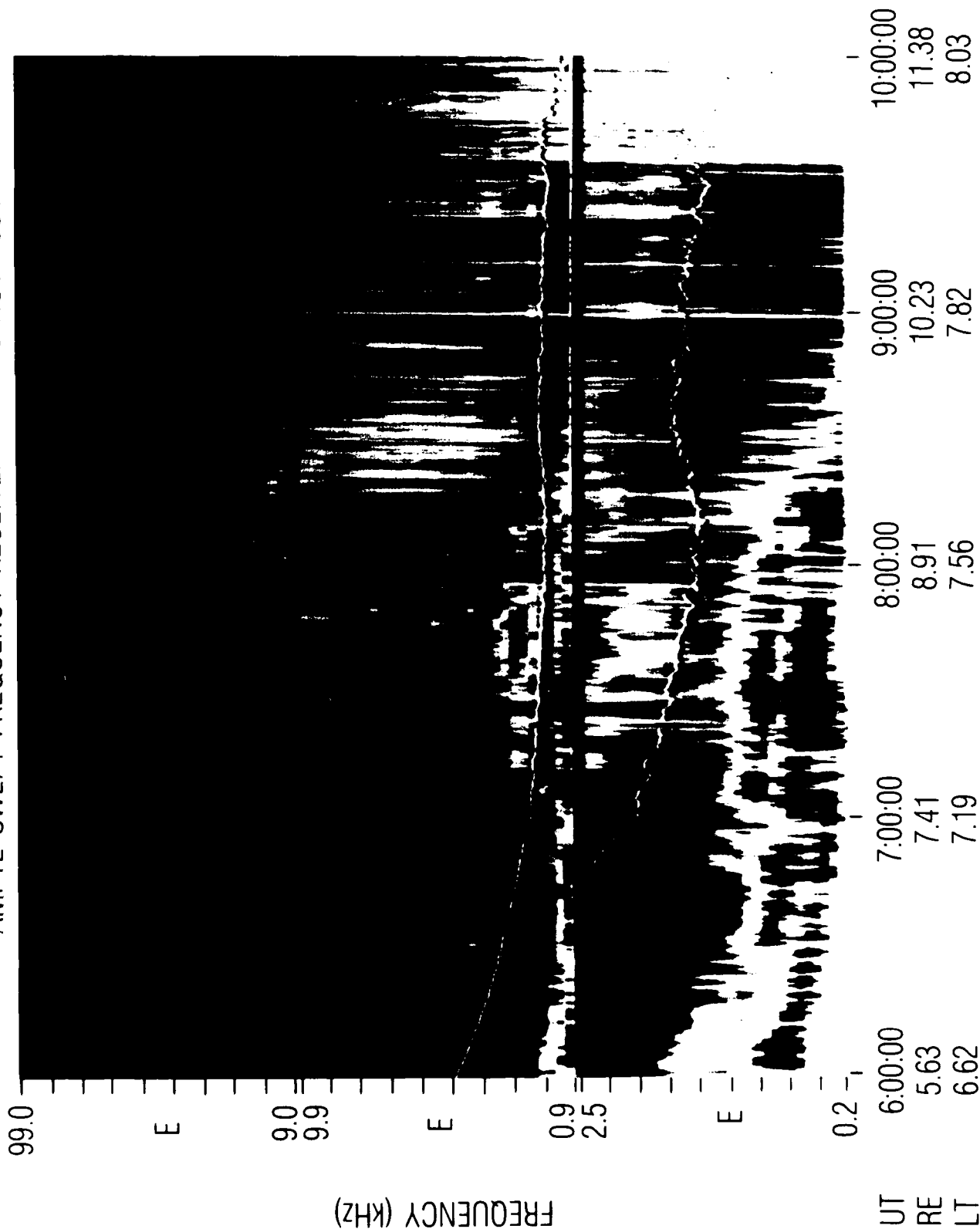
Fig. 5. Spectrogram of electric field spectral densities observed by AMPTE on November 10, 1984.

WAVE ELECTRIC FIELD SPECTRAL DENSITY
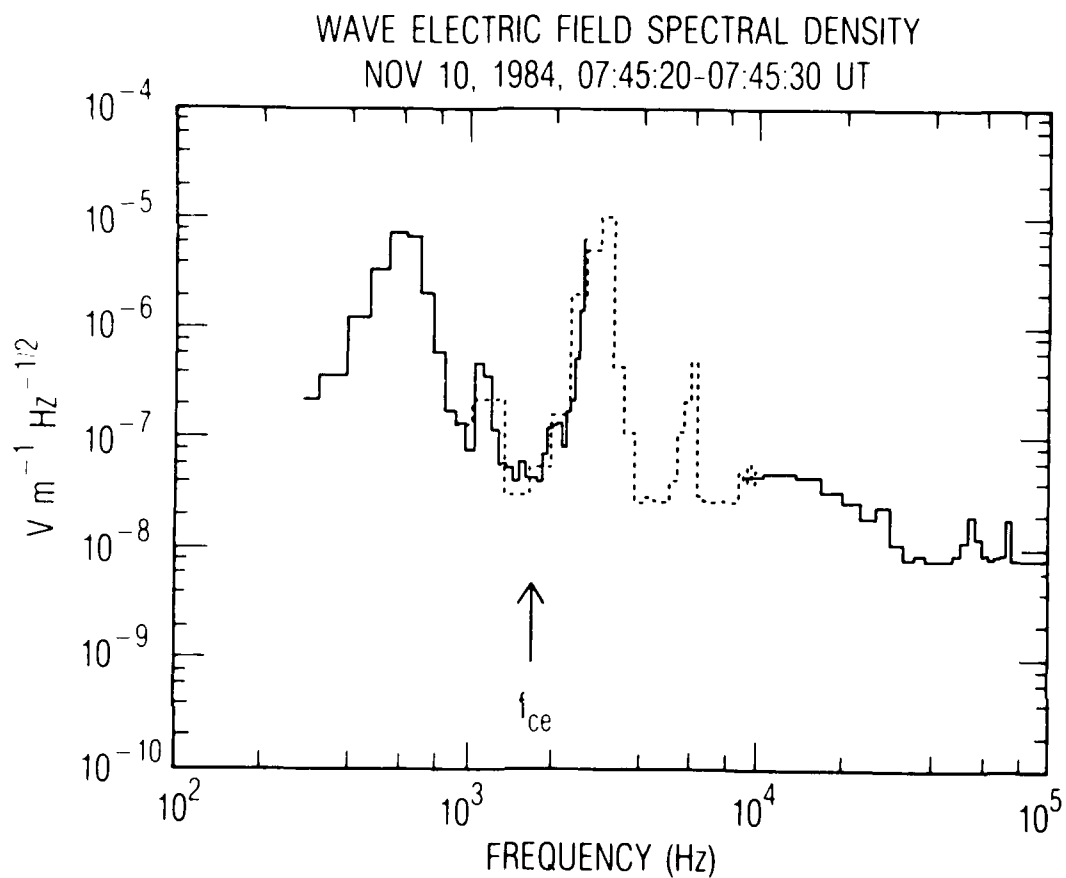NOV 10, 1984, 07:45:20-07:45:30 UT

Fig. 6. Spectral density of the electric field averaged over 10 s during the electron cyclotron emissions of November 10, 1984.

into a data base: 1) the time duration (0-10 min) that the spacecraft spent inside the magnetosphere with the SFR in the correct mode; 2) the time durations that the SFR detected ECH emissions of intensity greater than each of two threshold levels; 3) the date, Universal time, and the ephemeris of the spacecraft. The wave data were scrutinized manually to ensure the proper identification of the ECH emissions. The data base was then sorted to bin the records as a function of various parameters, including the spacecraft position and the geomagnetic index K_p. The frequency of occurrence of the ECH waves of intensities greater than the threshold was computed for a particular bin by dividing the total time that emissions of that intensity were detected by the total time that the spacecraft spent in that bin.

Because the magnetic latitude has such a pronounced effect on the occurrence of ECH emissions, we consider first the occurrence of the emissions as a function of magnetic latitude. Figures 7 and 8 show the coverage of the IRM and the occurrence frequency of the ECH emissions versus the dipole latitude of the spacecraft, respectively. In this analysis the data were sorted without regard to the local time of the IRM. Both figures are split into a low altitude plot in the bottom panel (McIlwain L parameter in the range 4-8) and the higher altitude data in the top panel (L ~ 8-12). The bottom panel of Figure 7 shows that the coverage is most tenuous at the small radii where the spacecraft is moving fastest, but is still above 5 h per 5° bin at latitudes from -15° to 10°. Note that each hour of coverage implies six intervals, each of 10-min duration. The high altitude coverage exceeds 10 h in the latitude range of -25° to 15°. The occurrence frequencies of the ECH emissions are shown in Figure 8 for two levels of spectral intensity. The plot labeled 'weak' corresponds to a threshold of 0.02 μV m^{-1} Hz$^{-1/2}$, which is approximately the minimum detectable intensity of the SFR. The 'strong' level is fifty times larger: 1 μV m^{-1} Hz$^{-1/2}$. These thresholds are presented as shades of blue and red on the intensity scale of Figures 1 and 5. The occurrence frequencies of emissions in the low altitude bins show pronounced effects of trapping

AMPTE IRM LATITUDINAL COVERAGE
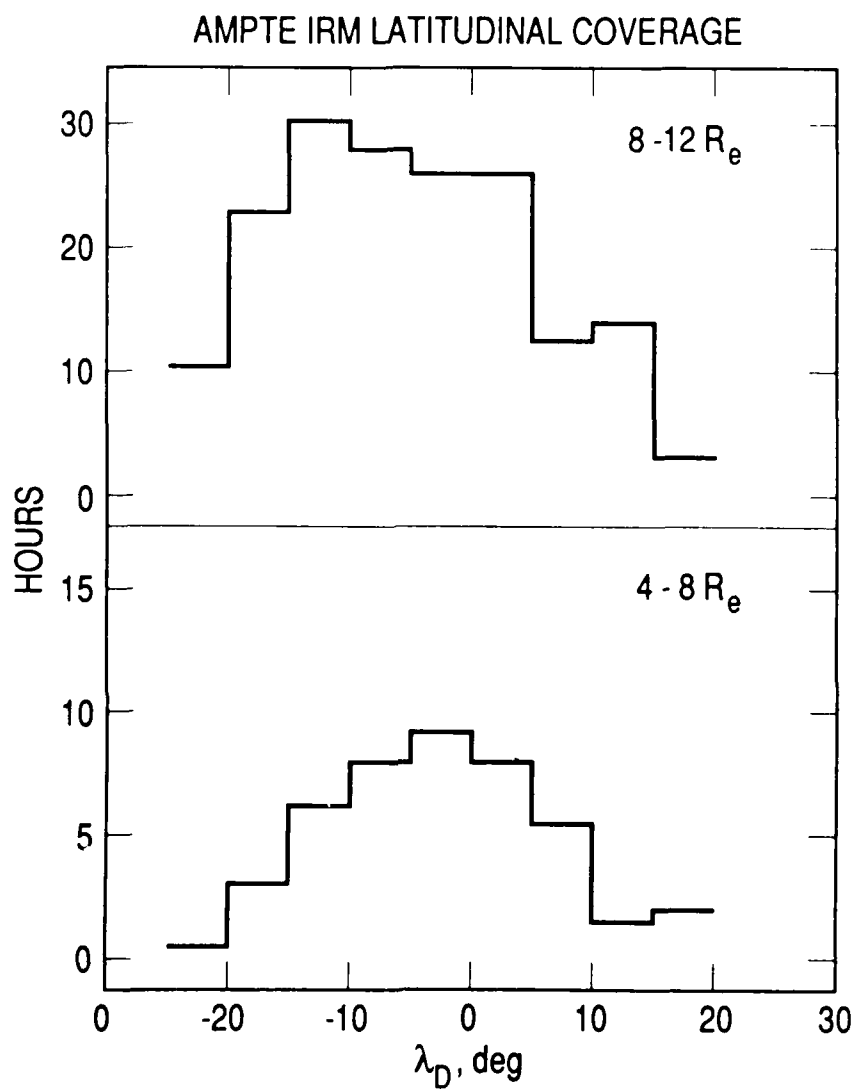
Fig. 7. Temporal coverage of the magnetosphere by the
AMPTE IRM instrument as a function of magnetic
dipole latitude for each of two radial bins.
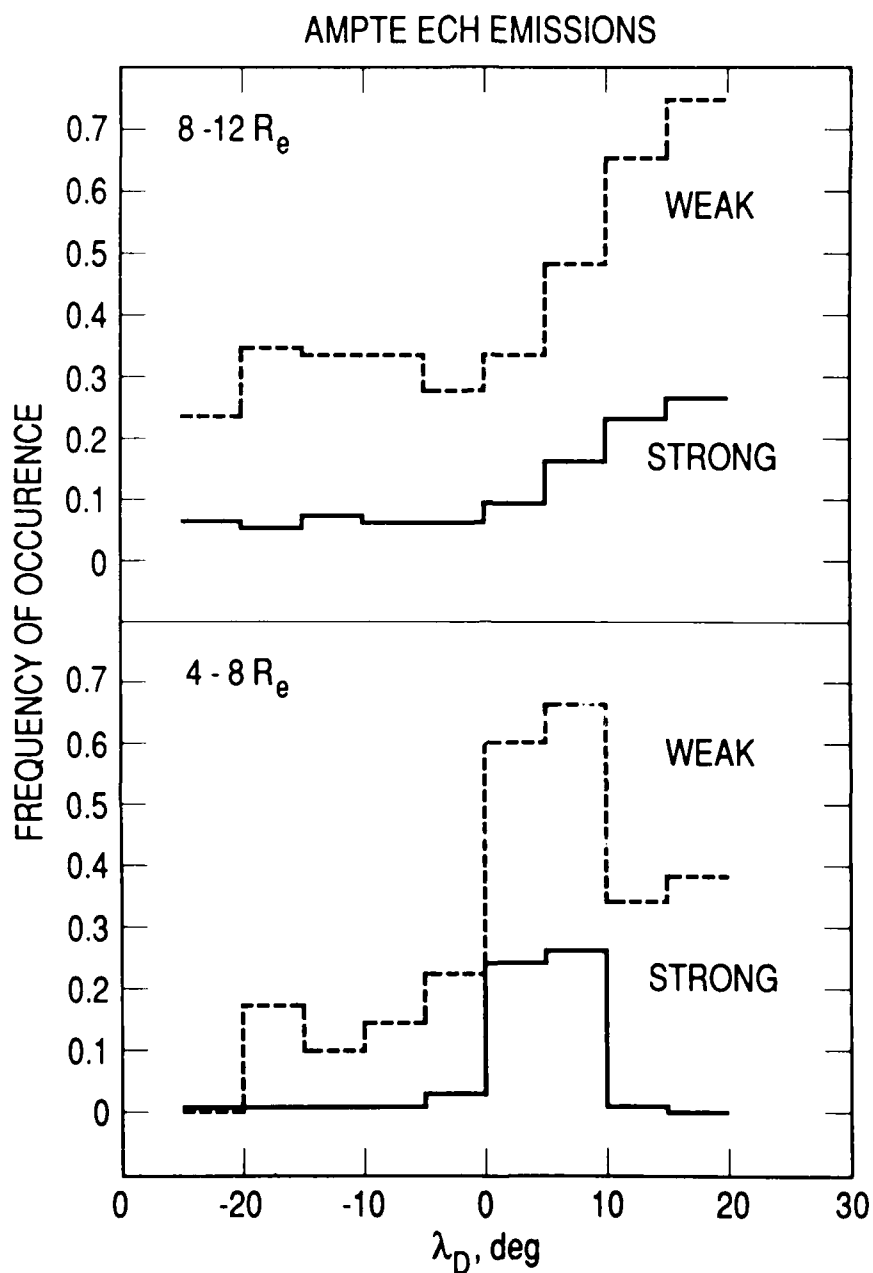
29

AMPTE ECH EMISSIONS

Fig. 8. Occurrence frequency of ECH wave emissions of spectral density greater than each of two thresholds: $0.02\ \mu V\ m^{-1}\ Hz^{-1/2}$ (labeled weak) and $1\ \mu V\ m^{-1}\ Hz^{-1/2}$ (strong) as a function of magnetic dipole latitude for each of two radial bins.

within latitudes in the range 0-10°. There is little difference in the distributions for the two thresholds except for the factor of 2.7 in the magnitude of the peak occurrence. The 5° offset in latitude of the peak is assumed to be due to inaccuracies in the magnetic field model used to compute the latitude. At the higher altitudes the evidence for trapping of the emissions near the equator is much less clear. There is an obvious enhancement of the occurrence frequency as the spacecraft exceeds 5° dipole latitude, although the coverage above 15° is minimal. One possible explanation for the high altitude distribution is that the magnetic field model becomes increasingly inaccurate at larger radii. This should cause a smearing of the distribution and a possible bias in latitude like that apparent in the lower panel. We note that the magnitudes of the peak occurrence frequencies at high altitudes for the two thresholds are nearly equal to the magnitudes of the low altitude peaks. There is certainly no evidence in the AMPTE data for a large increase in the occurrence of ECH emissions at high altitudes as suggested by Lyons [1984b].

The thresholds of the analysis of Figure 8 are extremely weak. In order to convert the threshold spectral intensity to an electric field amplitude that is relevant to the pitch angle diffusion, one must multiply by the square root of the bandwidth of the emissions. The emission bandwidth is difficult to determine accurately from the color spectrograms, but we can make some general estimates which will illustrate the tenuous nature of these waves. Based on the cases examined in detail using the methods presented in Figures 1-6, we have found that the majority of emissions have relative bandwidths of 10-20%. We assume a single emission at 1.5 f_{ce} which is stable in frequency for the time interval of the emission. Using the AMPTE data and the detailed spectral wave observations of Koons and Fennell [1984], we estimate that this assumption may lead to errors in the amplitude of only a factor of 2-3. Scaling the 20% bandwidth to the nominal equatorial value of 1.5 f_{ce} in a dipole magnetic field, the absolute bandwidths for the emissions can be crudely estimated to be 1000 Hz for L ~ 4-8 and 150 Hz for L ~ 8-12. These values convert the 'strong'

threshold of Figure 8 to 30 μV m^{-1} at L ~ 4-8 and 12 μV m^{-1} at L ~ 8-12, respectively. The limit of strong diffusion for 1-keV electrons was calculated by Belmont et al. [1983] to be 2 mV m^{-1} at L=7. This assumed that the waves were trapped within ±15° of the magnetic equator. Coroniti [1985] points out that this critical limit should scale with radial distance approximately as $L^{-7/2}$. This makes the limit in the range 1-14 mV m^{-1} for L ~ 4-8 and 0.3-1.0 mV m^{-1} for L ~ 8-12. The threshold amplitudes of Figure 8 are more than an order of magnitude below these estimates. For higher energy electrons, the amplitudes needed for strong diffusion are even larger because the limit also scales as $W^{3/4}$, where W is the electron energy [Coroniti, 1985].

Figures 9-11 show the results of the statistical study of the AMPTE data plotted as function of geocentric radial distance and local time. The range of the McIlwain radial parameter L from 4 to 20 is divided into four equal-width bins, and the local time is shown as eight bins of 3 h each. This analysis has been restricted to those observations taken at magnetic dipole latitudes in the range -10° to +10°. The spacecraft usually passes near the magnetic equator for only a short period on each orbit because of the high inclination (28°). For this reason it is impractical to limit the latitude to a range smaller than ±10°. Figure 9 presents the temporal coverage of the magnetic equator by the IRM spacecraft. The bins are shaded using the scale on the right side of the figure according to the total number of hours that the IRM spent in each region. Restricting the magnetic latitude greatly reduces the coverage, but it is still more than 8 hours for most bins above L ~ 8. Some of the bins at high altitudes have values much greater than 16 h, which saturates the scale in this figure. The coverage is most tenuous at low altitudes because of the high velocity of the IRM near perigee. The lowest coverage is in the two bins at L values of 4-8 and local times of 12-18 h, which each have 1-1.5 h of data.
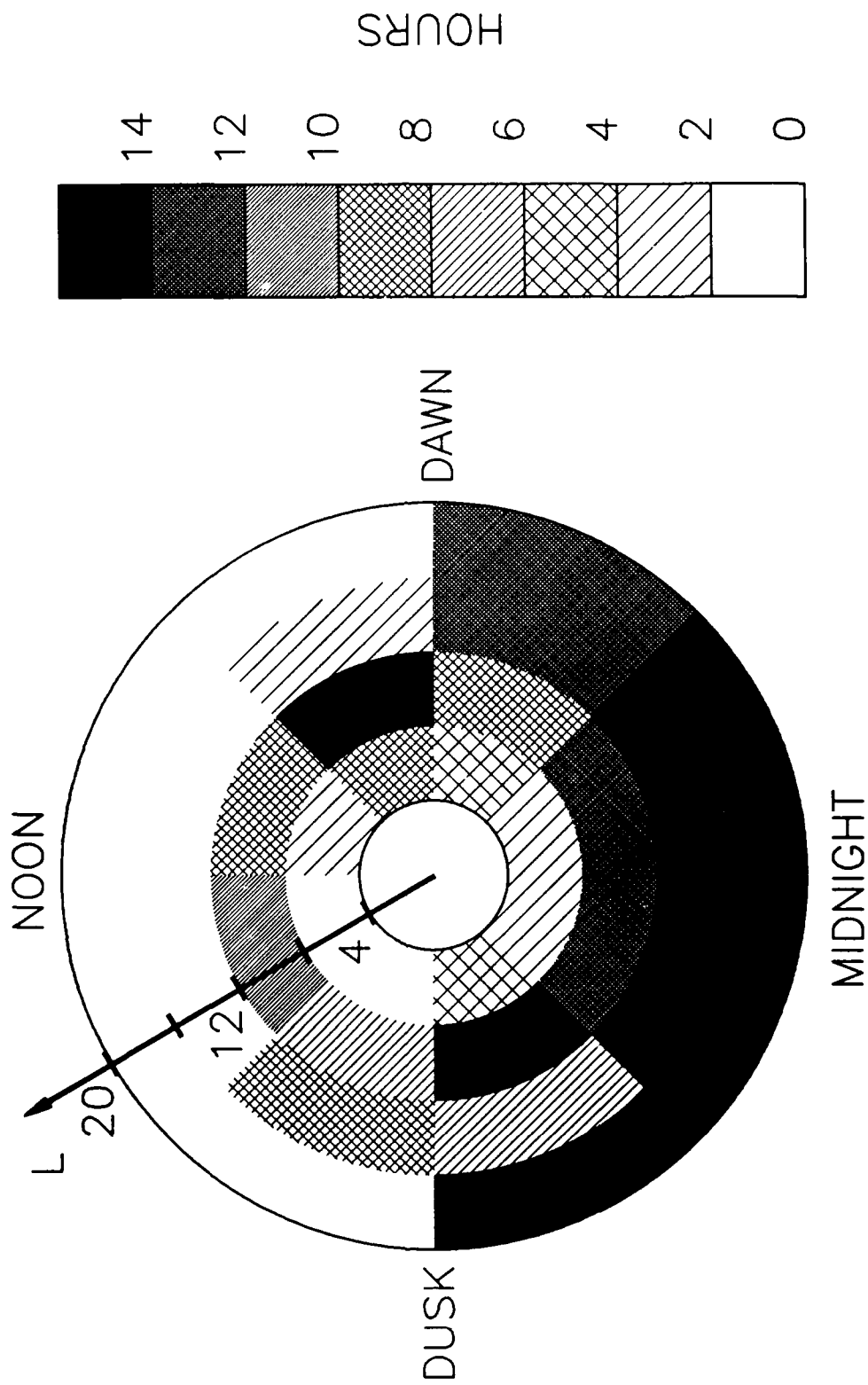
Fig. 9. Temporal coverage by the AMPTE IRM spacecraft of the magnetic equator (magnetic dipole latitudes in the range ±10°) as a function of L value and magnetic local time.

Figure 10 displays the frequency of occurrence of ECH emissions of intensity greater than 0.02 $\mu V\ m^{-1}\ Hz^{-1/2}$, which is approximately the minimum detectable level of the AMPTE instrument. ECH emissions were seen by the AMPTE instrument approximately 50-60% of the time in the region at 2100-0600 MLT and L values of 4-8. The occurrence frequencies for L ~ 8-12 are somewhat reduced because the data have been restricted to that within ±10° of the magnetic equator. If we used only the data at latitudes above 10°, the occurrence at L ~ 8-12 would increase to 60-70% and the rate at L ~ 4-8 would decrease in a manner consistent with Figure 8. The rate decreases to near 10-30% in the dusk half of the magnetosphere for all latitudes and radii. This pattern of radial-local time dependence is highly reminiscent of the occurrence statistics of electromagnetic ELF chorus as shown by Tsurutani and Smith [1977] and Tsurutani et al. [1979]. These whistler-mode emissions are thought to be closely related to the enhanced, anisotropic fluxes of energetic electrons because their region of occurrence closely resembles the drift paths of such particles. The two instabilities that are assumed to generate the chorus emissions and the ECH emissions both depend on the presence of anisotropic electron distributions, so it is not surprising that the occurrence patterns of the two types of waves appear similar. The ECH generation mechanisms usually require anisotropy at lower energies than those for chorus, so the patterns should exhibit some differences. However, these effects are probably too small to be resolvable with the AMPTE data set.

The occurrence rates of emissions of intensity greater than 1 $\mu V\ m^{-1}$ $Hz^{-1/2}$ are shown in Figure 11. The more intense emissions exhibit the same general pattern as those of Figure 9, but at lower levels of occurrence (note the reduction of the scale). The maximum level of occurrence is reduced by a factor of 2.5 for a fifty-fold increase in the threshold, which is consistent with Figure 8. The radial bins for this analysis are rather large, but the sparse nature of the data near perigee preclude a radial bin size of less than four. However, a similar analysis was performed using bins of identical size but offset (L ~ 6-10, 10-14, and
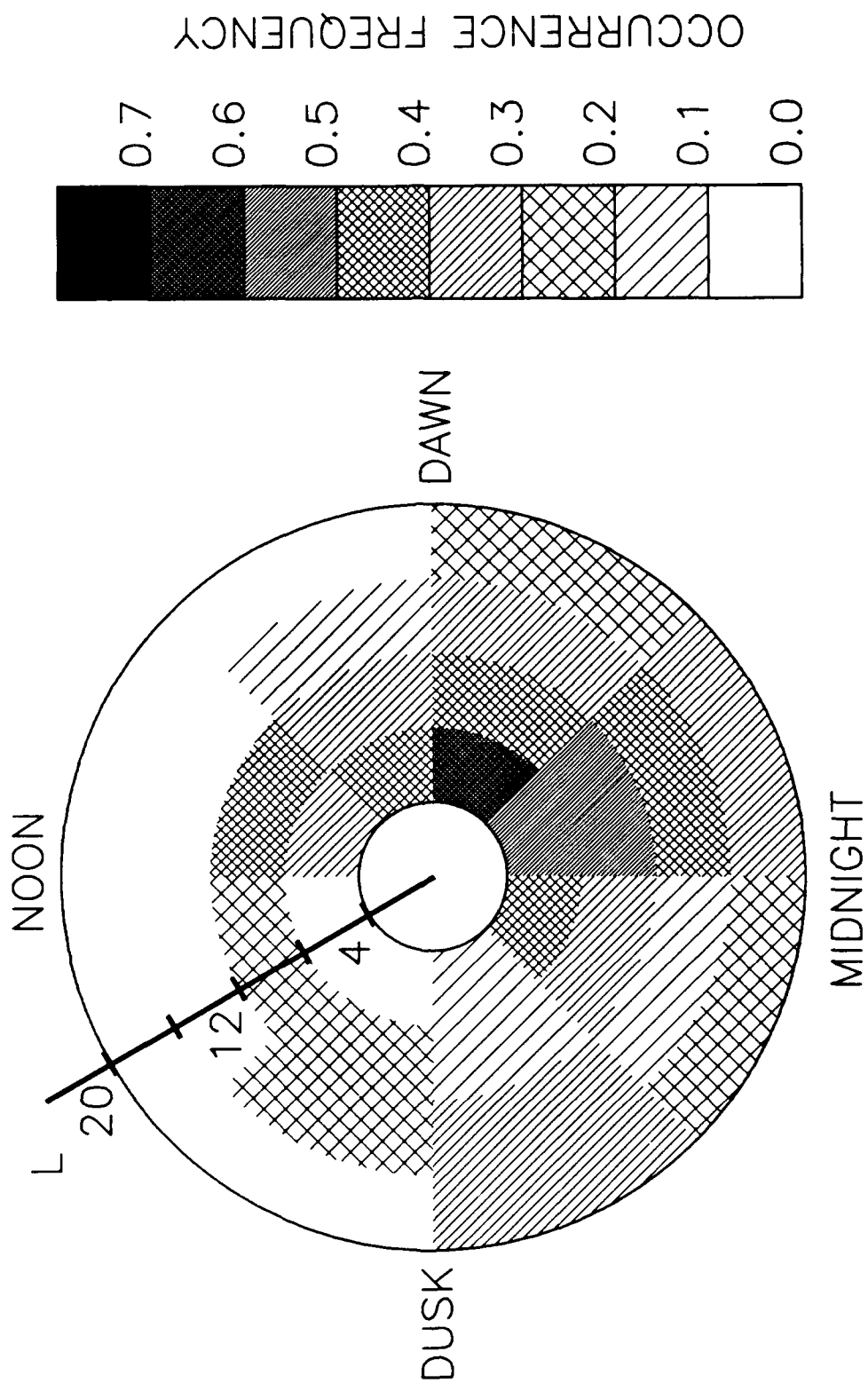
Fig. 10. Occurrence frequency of ECH waves of spectral density greater than $0.02 \ \mu V \ m^{-1} \ Hz^{-1/2}$ as a function of L and magnetic local time of the AMPTE IRM spacecraft.
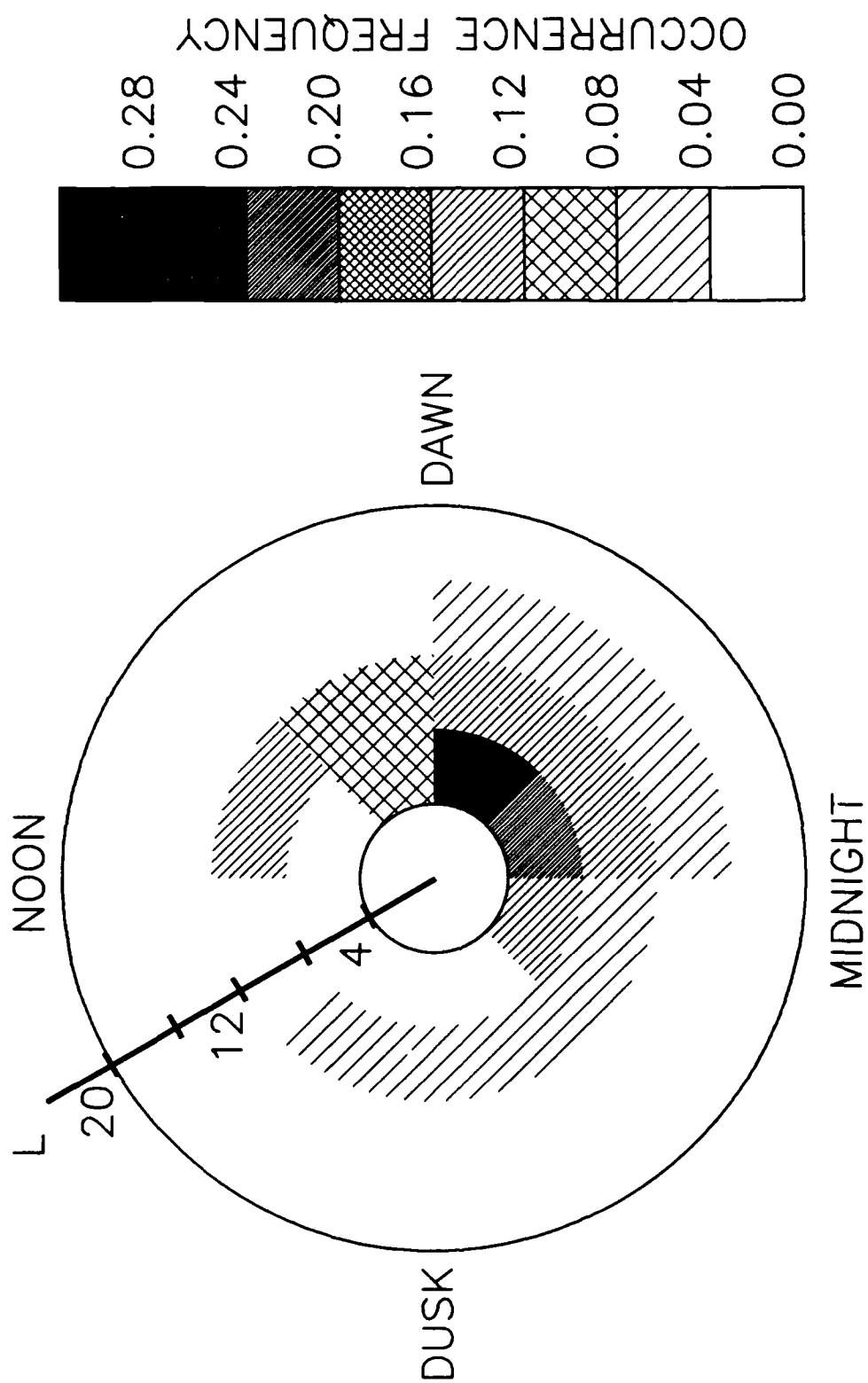
Fig. 11. Occurrence frequency of ECH waves of spectral density greater than 1 μV m^{-1} Hz$^{-1/2}$ as a function of L and local time of the AMPTE IRM spacecraft.

36

14-20) from those displayed in Figures 7-11. The radial-local time patterns produced with the offset bins were very similar to Figures 7-11 within the statistical significance of the data. This analysis included the data for all levels of geomagnetic activity. If the data are sorted into quiet ($K_p < 3$) and active ($K_p > 3$) cases, the latitudinal and radial-local time patterns remain much the same, except the levels of occurrence for the active periods are approximately two times larger than those of the quiet bins. There is no evidence in the AMPTE observations for a dependence of the wave occurrence on K_p similar to that found by Gussenhoven et al. [1983] in the auroral precipitation data.

Because of the sparse nature of the IRM coverage at geocentric radii below 8 R_e, we have supplemented the IRM survey with data from the SCATHA spacecraft. An analysis which is very similar to the IRM survey was performed using the wideband analog data from the VLF receiver on SCATHA. Wideband data were collected during 1979 and 1980 and were limited to 1-2 h per day. An atlas of VLF spectrograms from each wideband data acquisition during 1979 has been compiled by Koons et al. [1981]. This collection contains examples of each type of signal detected during a given data acquisition. For example, if electrostatic cyclotron harmonic waves were detected at the beginning of an acquisition and chorus at the end of the acquisition, there would be two photographs in the atlas. A data base was compiled from the atlas, with one entry for each acquisition. The data base contains logical fields for the occurrence of ECH waves, chorus, and hiss. Because of the crude time resolution of this survey, the magnitudes of the occurrence frequency are only rough estimates. Since the assessment of the occurrence was made from the spectrograms, the sensitivity is just above the noise level of the instrument, which is 0.5 μV m^{-1} $Hz^{-1/2}$. The same assumptions that were made for the AMPTE data can be used to estimate the bandwidth of the emissions detected by SCATHA. The above spectral intensity corresponds to an amplitude of 16 μV m^{-1} for ECH emissions at $L \sim 4-8$.

The frequency of occurrence of ECH emissions detected by the SCATHA wideband receiver is shown in the bottom panel of Figure 12 as a function of the absolute magnetic dipole latitude. The top panel shows that the temporal coverage of the spacecraft is more than adequate out to latitudes of 20°. The occurrence of ECH emissions exhibits a substantial trapped
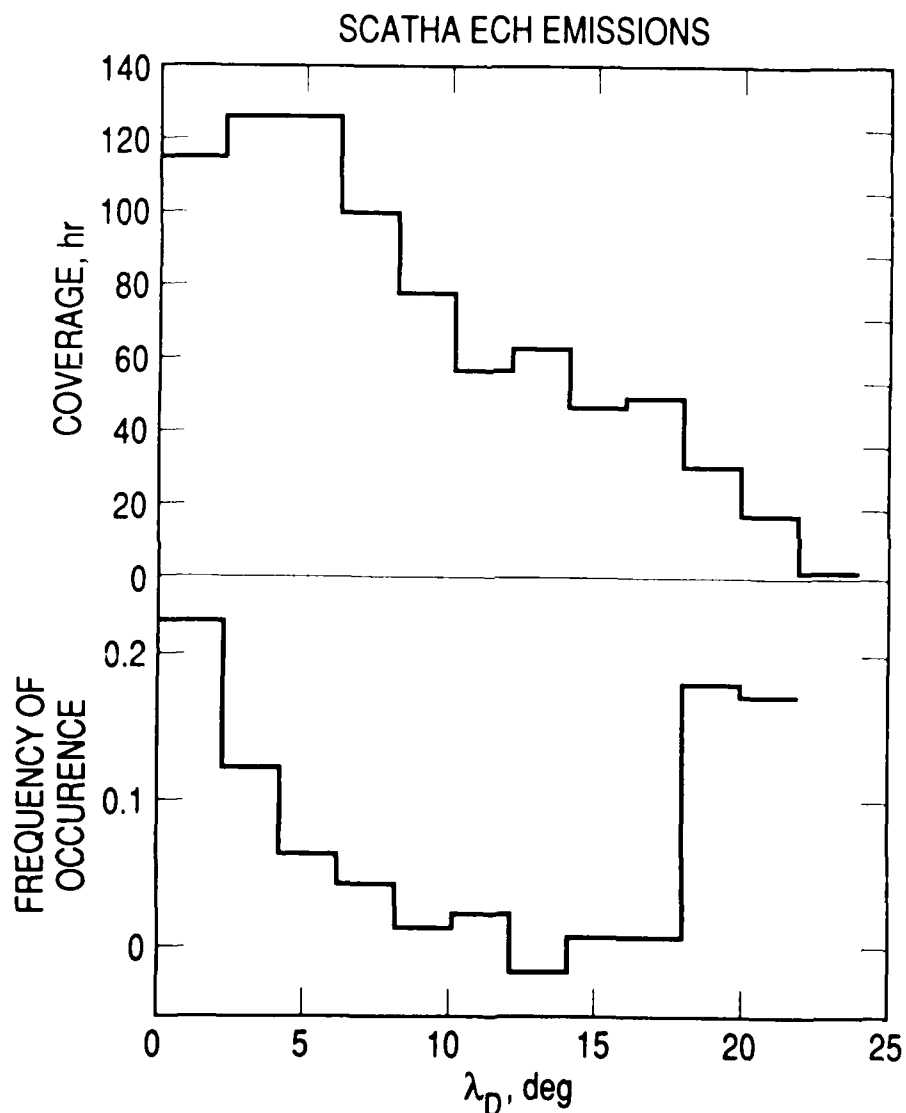

Fig. 12. Frequency of occurrence of ECH emissions and the temporal coverage of the SCATHA wideband data as a function of the magnetic dipole latitude of the spacecraft.

38

component below 5°, but there seems to be an isolated population of emissions at 18-20°. These high latitude emissions do not exhibit any clear pattern with respect to location or geomagnetic activity. No explanation of the high latitude emissions is obvious, but the number of cases is fairly small, and we intend to investigate them in more detail.

Figures 13 and 14 display the SCATHA wideband survey results in a format similar to that of Figure 9. This analysis has been restricted to that data at latitudes below 10°. The range of L from 5 to 8 is divided into three equal bins, and the magnetic local time range is divided into eight equal bins. Figure 13 shows that the coverage is greater than 15 h for most bins. Figure 14 shows the frequency of occurrence of the ECH emissions detected by the SCATHA wideband channel plotted as a function of L and magnetic local time. There is a clear maximum in the frequency of occurrence on the night side from 2100 to 0600 LT. The frequency of occurrence never exceeds 60% over the entire region covered by SCATHA.

The probability of occurrence of the ECH emissions as a function of latitude was shown in Figure 10, using the AMPTE data. We now address the variation in amplitude of ECH emissions with latitude, using an analysis of the SCATHA narrowband data. Occasionally SCATHA spends several tens of minutes very close to the magnetic equator. Ten intervals in 1979 were identified in which the satellite spent more than 30 min within 0.1° of the magnetic equator. These periods were located at a variety of local times and radii within the range of Figure 11. ECH emissions were detected only during the two intervals within 2 h of local midnight. This result is in general agreement with the statistical study presented in this report. The narrowband data and the magnetic latitude of the satellite during these two intervals are shown in Figure 15. These data represent the largest-amplitude ECH waves observed by the SCATHA satellite in 2 yr of operation. The maximum wave amplitude observed during these intervals was 1.25 mV m^{-1} in a channel with a bandwidth of 345 Hz at 2.3 kHz. This level corresponds to a spectral density of 80 μV m^{-1} Hz$^{-1/2}$, assuming a single emission of 10% relative bandwidth in the center of the channel. We estimate that the

39

OCCURRENCE FREQUENCY
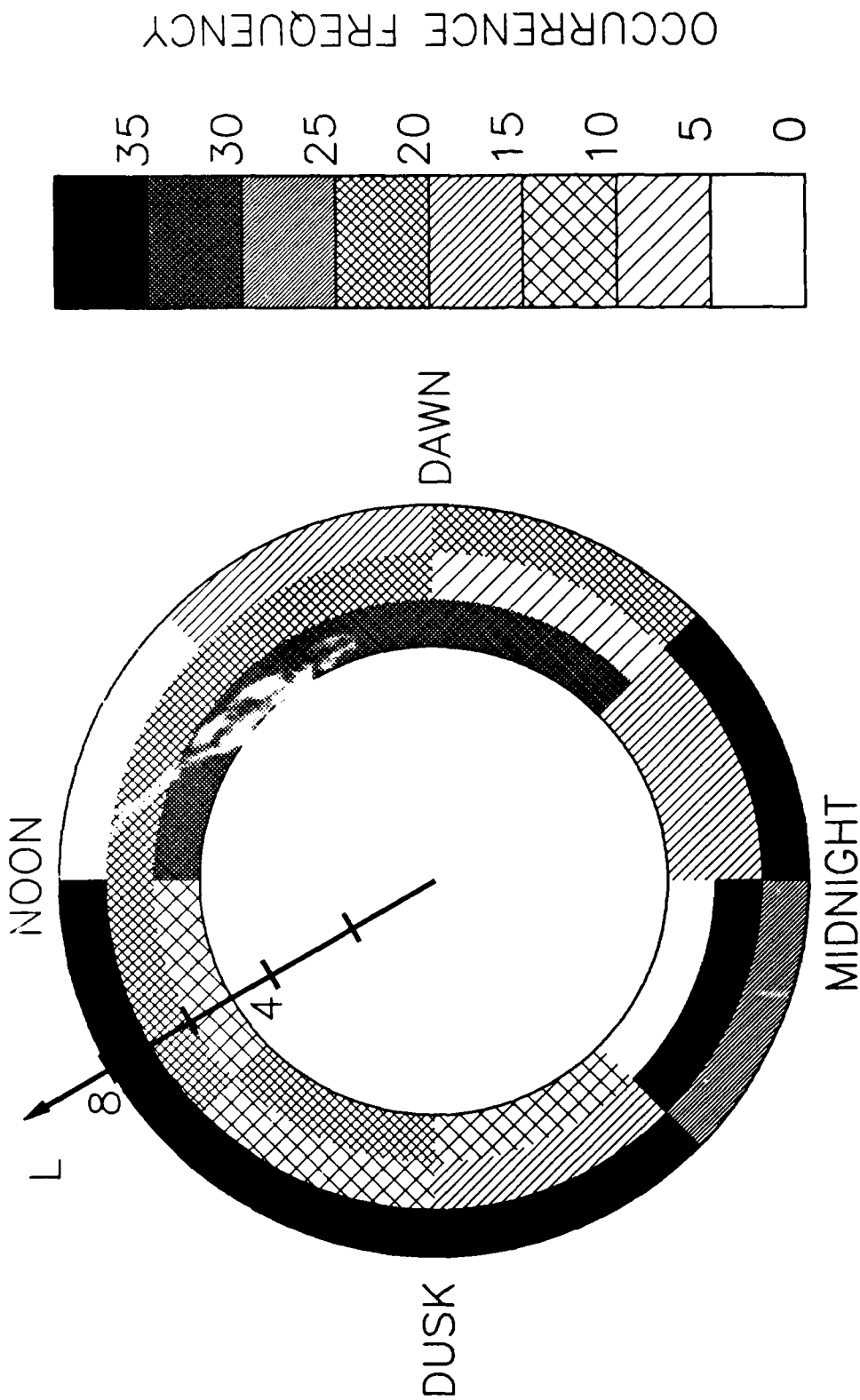
Fig. 13. Temporal coverage of the magnetic equator by the SCATHA satellite as a function of L and magnetic local time. The range of L from 5 to 8 is divided into three equal bins, and the local time is divided into eight equal bins.
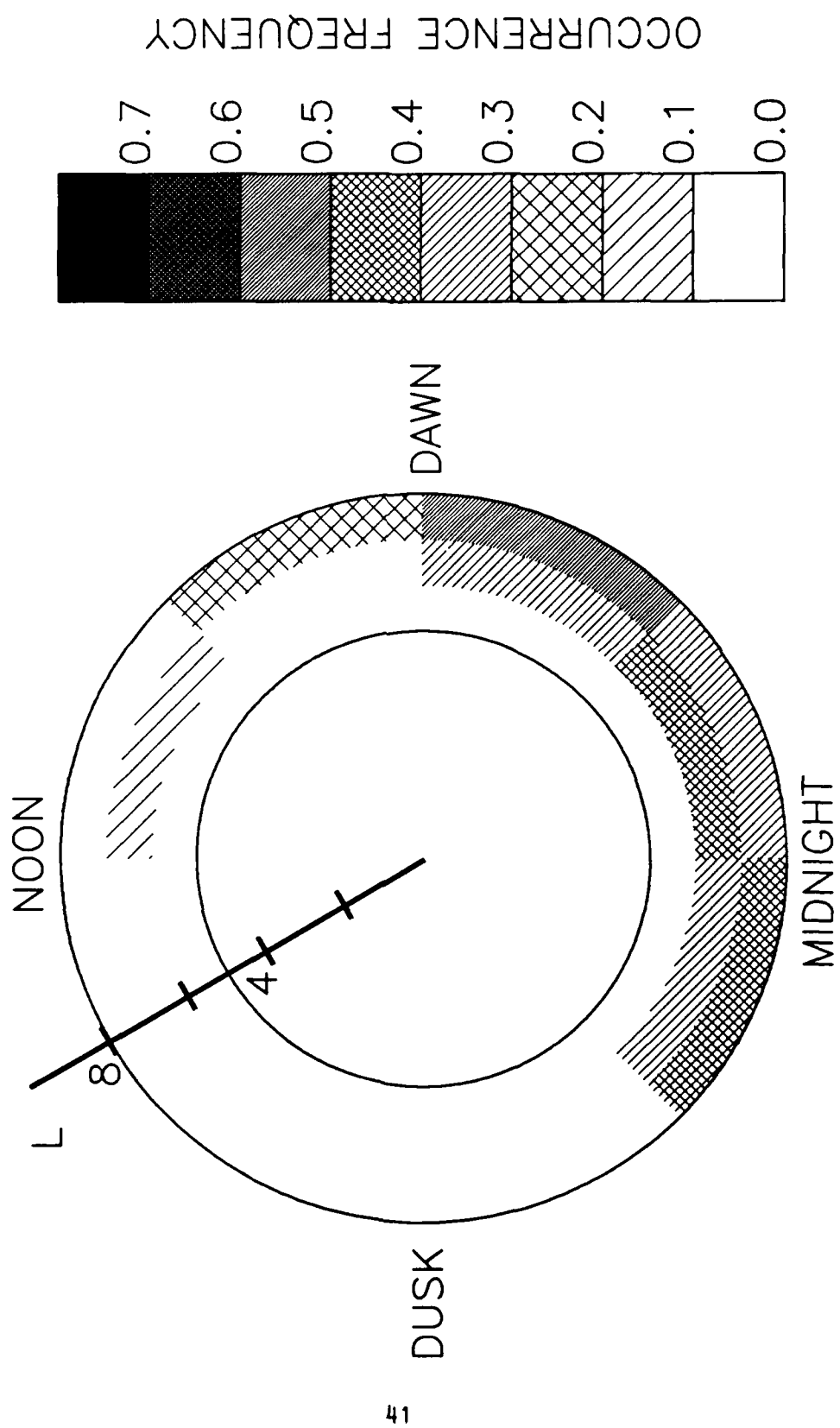
Fig. 14. Frequency of occurrence of the ECH emissions detected in the SCATHA broadband data as a function of L and magnetic local time.

41
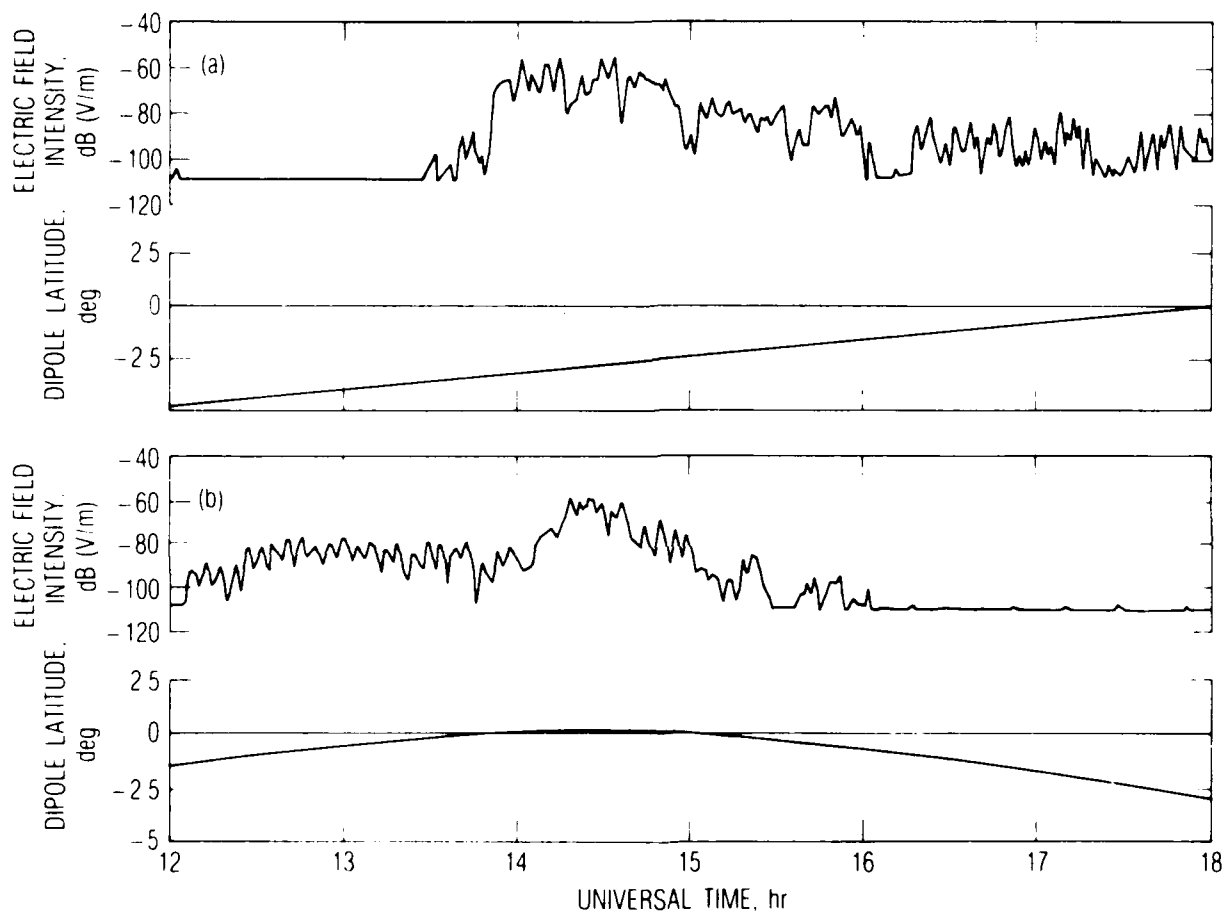
Fig. 15. Narrowband electric field amplitudes measured by the SCATHA VLF receiver during two intervals in which the satellite was near the magnetic equator. Case (a) occurred on April 16, 1979, and (b) was observed on September 2, 1979.

amplitude could be in error by a factor of 3-5 because of the narrow width of the frequency channel and the possible frequency variations of the emissions. The variation of the wave amplitude in Figure 13a does not seem to be simply related to the dipole latitude of the satellite. This effect could be the result of several processes, including temporal variations of the wave generation mechanism and the validity of the magnetic field model used to compute the dipole latitudes. Figure 13b shows the expected maximum in wave amplitude at the magnetic equator. The amplitude increases by an order of magnitude to approximately 1 mV m^{-1} for latitudes less than 0.25°. But this extremely tight trapping of the waves around the equator causes the strong diffusion limit for 1-keV electrons to increase to approximately 10 mV m^{-1}. These rather crude estimates tend to confirm the notion that the ECH emissions at magnetic latitudes even very near zero are weak compared to the levels needed for strong diffusion in such a confined equatorial region.

The results of the survey of ECH emission, using the data from the AMPTE IRM and SCATHA spacecraft, are summarized in Table 1. The result of the GEOS survey of Belmont et al. [1983] are also shown for comparison.

Table 1. Occurrence of ECH Wave Emissions

Spacecraft	L	λ_D (degrees)	E_t (mV m^{-1})	Occurrence
GEOS-2	6.6	-3	0.1	0.12
	6.6	-3	1.0	0.02
AMPTE-IRM	4-8	±10	0.035	0.27
	8-12	±10	0.012	0.26
SCATHA	5-8	±5	0.016	0.45

The ranges of the radius, and magnetic latitude are listed with the threshold electric-field amplitude of the survey. The occurrence frequencies of the emission have been taken from the latitudinal analyses of Figures 8 and 12. The comparison of this survey with the results of Belmont et al. [1983] is difficult because of the different amplitude thresholds and latitude ranges. Perhaps due to the inclination of the orbit, only four cases of emissions with amplitudes above 1 mV m^{-1} were observed by the AMPTE instrument in two years of operation. Raising the thresholds for the AMPTE survey to strong diffusion levels would obviously produce a null result. The weak emissions seen by the IRM instruments seem inconsistent with the early observations of 10 mV m^{-1} waves by OGO 5 [Kennel et al., 1970; Fredricks and Scarf, 1973] and Imp 6 [Shaw and Gurnett, 1975]. But Gurnett et al. [1979] report that ISEE-1 detected ECH emissions in a range of amplitude closer to the IRM results (several hundred mV m^{-1} to about one mV m^{-1}). The lack of strong waves in the AMPTE data does imply that, if large ECH emissions exist for radii beyond geosynchronous orbit, they are then trapped at extremely small latitudes. For this reason, the results of the AMPTE survey tend to confirm Belmont et al. [1983].

IV. CONCLUSIONS

The statistical study of the plasma wave data from the AMPTE-IRM and
SCATHA satellites has shown that the occurrence of ECH wave emissions is
comparable to that previously reported by the GEOS investigators. We found
that ECH emissions were observed most often in the 0300-0600 LT sector of
the magnetosphere at geocentric distances of 4-8 R_e. In this region ECH
emissions of amplitude exceeding 12 $\mu V\ m^{-1}$ were detected 60% of the time
and emissions exceeding 35 $\mu V\ m^{-1}$ were detected only 25% of the time.
Between local noon and midnight, ECH emissions were detected less than 20%
of the time. The emissions of amplitude greater than the stronger
threshold cited above tended to be confined to within ±10% of the magnetic
equator. The level of geomagnetic activity seems to have little effect on
the pattern of ECH occurrence other than generally increasing the number of
emissions. There was no evidence for a large number of strong emissions at
altitudes beyond geosynchronous orbit as speculated by Lyons [1984b]. We
conclude that the assertion of Belmont et al. [1983] is essentially
correct: the occurrence and intensity of ECH wave emissions is too small
to account for the continuous precipitation of magnetospheric electrons in
the diffuse aurora. A better statistical study of the diffuse electron
precipitation is needed to quantify this discrepancy. The results of this
study should be compared to the occurrence frequency for a given level of
precipitated electron flux.

The implications of this work for the cause of the diffuse aurora can
take several forms. One possibility is that the process of quasilinear
particle diffusion by ECH waves may be much more efficient than previously
estimated. The large amount of laboratory and computer simulation work
that has been done to validate the theory makes this possibility unlikely
unless one of the underlying assumptions has been violated. The quasilin-
ear theory assumes small amplitudes and random phases for the waves. The
first assumption is certainly satisfied by the data. The question of the
coherence of the waves should be addressed by an observational study of the

45

ECH emissions and possibly a computer simulation of the particle scattering process.

If we accept the implication that ECH are not connected to the diffuse electron precipitation, then we may search for other waves which might be responsible. Unfortunately, there exist no known waves in the equatorial magnetosphere of the required intensity which occur on a semicontinuous basis. The remaining possibility is that the precipitation is caused by a wave-particle interaction at low or middle altitudes on the auroral field lines. But a second process may then be required to supply electrons from the equator to the lower-altitude interaction region.

One of the main arguments for an equatorial interaction region is that particle instruments observe a large radial gradient in the electron temperature at the inner edge of the plasma sheet. Kennel and Ashour-Abdalla [1982] infer from this that nearly all the plasma sheet electrons must be scattered into the loss cone, which can be done only from the equator. However, according to plasma convection theories using the single particle approximation [for example, Cowley and Ashour-Abdalla, 1975], the profiles of observed plasma bulk parameters may, at least for some periods, be simulated quite well by Alfven layer effects alone. Thus, precipitation may not be as important to the observed gradient as originally thought. Several computer simulations of the magnetospheric convection process have attempted to take into account the effects of particle precipitation by wave-particle interactions [Fontaine and Blanc, 1983; Fontaine et al., 1985, Harel et al., 1981]. But all these calculations use the strong diffusion limit or a simple modification of it to approximate the level of precipitation. Many researchers believe that the loss cone in the near-earth plasma sheet is always "quasi-filled," yet there has never been an observational study of this assumption as noted by Belmont et al [1983]. Most particle instruments in the 0.01-20 keV energy range have insufficient angular resolution to investigate the loss cone at high altitudes without substantial deconvolution analysis.

46

Until the particular mechanism which is causing the precipitation can be identified, it will be difficult to access quantitatively its effects on the magnetospheric system. It seems that the only method of solving the diffuse aurora problem is more coordinated studies of the particles and the wave fields at several points along a geomagnetic field line.

REFERENCES

Ashour-Abdalla, M., and C. F. Kennel, Diffuse auroral precipitation, J. Geomag. Geoelectr., 3C, 239-255, 1978.

Barbosa, D. D., On the convective properties of magnetospheric Bernstein waves, J. Geophys. Res., 85, 2341-2345, 1980.

Barbosa, D. D., Electrostatic wave propagation and trapping near the magnetic equator, Ann. Geophys., 3, 63-72, 1985.

Belmont, G., D. Fontaine, and P. Canu, Are equatorial electron cyclotron waves responsible for diffuse auroral precipitation? J. Geophys. Res., 88, 9163-9170, 1983.

Belmont, G., D. Fontaine, and P. Canu, Reply, J. Geophys. Res., 89, 7591-7592, 1984.

Birmingham, T. J., Pitch angle diffusion in the Jovian magnetodisc, J. Geophys. Res., 89, 2699-2707, 1984.

Canu, P., Étude des ondes électrostatiques à l'aide du satellite GEOS-2, Thesis, Pierre & Marie Curie University, Paris, France, 1982.

Coroniti, F. V., Space plasma turbulent dissipation: reality or myth? Space Sci. Rev., 42, 399-410, 1985.

Cowley, S. W. H., and M. Ashour-Abdalla, Adiabatic plasma convection in a dipole field: Variation of plasma bulk parameters with L, Planet. Space Sci., 23, 1527-1549, 1975.

Deehr, C. S., J. D. Winningham, F. Yasuhara, and S.-I. Akasofu, Simultaneous observations of discrete and diffuse auroras by the Isis 2 satellite and airborne instruments, J. Geophys. Res., 81, 5527-5535, 1976.

Engel, J., and C. F. Kennel, Effect of parallel refraction on magnetospheric upper hybrid waves, Geophys. Res. Lett., 11, 865-868, 1984.

Engel, J., and C. F. Kennel, The effects of density gradients on the convective amplification of upper hybrid waves in the magnetosphere, Planet. Space Sci., 33, 1331-1357, 1985.

Fairfield, D. H. and A. F. Viñas, The inner edge of the plasma sheet and the diffuse aurora, J. Geophys. Res., 89, 841-854, 1984.

Fennell, J. F., Description of P78-2 (SCATHA) satellite and experiments, The IMS Source Book, edited by C. T. Russell and D. J. Southwood, 65-81, Amer. Geophys. Union, Wash., D.C., 1982.

Fontaine, D., and M. Blanc, A theoretical approach to the morphology and the dynamics of diffuse auroral zones, J. Geophys. Res., 88, 7171-7184, 1983.

Fontaine, D., M. Blanc, L. Reinhart, and R. Glowinski, Numerical simulations of the magnetospheric convection including the effects of electron precipitation, J. Geophys. Res., 90, 8343-8360, 1985.

Fontaine, D., S. Perraut, N. Cornilleau-Wehrlin, B.Aparicio, J. M. Bosqued, D. Rodgers, Coordinated observations of electron energy spectra and electrostatic cyclotron waves during diffuse auroras, Ann. Geophys., 4, 405-412, 1986.

Fredricks, R. W., and F. L. Scarf, Recent studies of magnetospheric electric field emissions above the electron gyrofrequency, J. Geophys. Res., 78, 310-314, 1973.

Gough, M. P., P. J. Christiansen, and E. J. Gershuny, ES wave morphology near geostationary orbit, Adv. Space Res., 1, 337-343, 1981.

Gurnett, D. A., R. R. Anderson, F. L. Scarf, F. W. Fredricks, and E. J. Smith, Initial results from the ISEE-1 and -2 plasma wave investigation, Space Sci. Rev., 23, 103-122, 1979.

Gussenhoven, M. S., D. A. Hardy, and N. Heinemann, Systematics of the equatorward diffuse auroral boundary, J. Geophys. Res., 88, 5692-5708, 1983.

Gustafsson, G., Latitude and local time dependence of precipitated low-energy electrons at high latitudes, J. Geophys. Res., 78, 5537-5552, 1973.

Hausler, B., R. R. Anderson, D. A. Gurnett, H. C. Koons, R.H. Holzworth, O. H. Bauer, R. Treumann, K. Gnaiger, D.Odem, W. B. Harbridge, and F. Eberl, The plasma wave instrument on board the AMPTE satellite, IEEE Trans. Geosci. Remote Sensing, GE-23, 267-273, 1985.

Harel, M., R. A. Wolf, P. H. Reiff, R. W. Spiro, W. J. Burke, F. J. Rich, and M. Smiddy, Quantitative simulation of a magnetospheric substorm, 1. model logic and overview, J. Geophys. Res., 86, 2217-2241, 1981.

Horwitz, J. L., S. Menteer, J. Turnley, J. L. Burch, J. D. Winningham, C. R. Chappell, J.D. Craven, L. A. Frank, and D. W. Slater, Plasma boundaries in the inner magnetosphere, J. Geophys. Res., 91, 8861-8882, 1986.

Kennel, C. F., Consequences of a magnetospheric plasma, Rev. Geophys., 7, 379-419, 1969.

Kennel, C. F., F. L. Scarf, R. W. Fredricks, J. H. McGhee, and F. V. Coroniti, VLF electric field observations in the magnetosphere, J. Geophys. Res., 75, 6136-6152, 1970.

Kennel, C. F., and M. Ashour-Abdalla, Electrostatic waves and the strong diffusion of magnetospheric electrons, Magnetospheric Plasma Physics, edited by A. Nishida, 245-344, Center for Academic Publications, Tokyo, Japan, 1982.

Koons, H. C., and J. F. Fennell, Particle and wave dynamics during plasma injection, J. Geophys. Res., 88, 6221-6229, 1983.

Koons, H. C., and J. F. Fennell, Fine structure in electrostatic emission bands between electron gyrofrequency harmonics, J. Geophys. Res., 89, 3015-3018, 1984.

Koons, H. C., R. J. Maulfair, and J. C. Kordan, An atlas of spectrograms from the VLF receiver aboard the SCATHA (P78-2) spacecraft, ATR-81(7954)-2, The Aerospace Corp., El Segundo, Calif., Sept. 1981.

Lühr, H., N. Klöcker, W. Oelschlägel, B. Häusler, and M. Acuna, The IRM fluxgate magnetometer, IEEE Trans. Geosci. Remote Sensing, GE-23, 259-261, 1985.

Lui, A. T. Y., and C. D. Anger, A uniform belt of diffuse auroral emission seen by the ISIS-2 scanning photometer, Planet. Space Sci., 21, 799-809, 1973.

Lui, A. T. Y., P. Perreault, S.-I. Akasofu, and C. D. Anger, The diffuse aurora, Planet. Space Sci., 21, 857-861, 1973.

Lyons, L. R., Electron diffusion driven by magnetospheric electrostatic waves, J. Geophys. Res., 79, 575-580, 1974.

Lyons, L. R., Electron energization in the geomagnetic tail current sheet, J. Geophys. Res., 89, 5479-5487, 1984a.

Lyons, L. R., Comment on "Are equatorial electron cyclotron waves responsible for diffuse auroral electron precipitation?" by G. Belmont, D. Fontaine, and P. Canu, J. Geophys. Res., 89, 7589, 1984b.

Lyons, L. R., and J. F. Fennell, Characteristics of auroral electron precipitation on the morningside, J. Geophys. Res., 91, 11225-11234, 1986.

Meng, C.-I., B. Mauk, and C. E. McIlwain, Electron precipitation of evening diffuse aurora and its conjugate electron fluxes near the magnetospheric equator, J. Geophys. Res., 84, 2545-2558, 1979.

Newell, P. T., and C.-I. Meng, Energy dependence of the equatorward cutoffs in auroral electron and ion precipitation, J. Geophys. Res., 92, 7519-7530, 1987.

Scarf, F. L., R. W. Fredricks, C. F. Kennel, and F. V. Coroniti, Satellite studies of magnetospheric substorms on August 15, 1968, J. Geophys. Res., 78, 3119-3130, 1973.

Schumaker, T. L., M. S. Gussenhoven, D. A. Hardy, and R. L. Carovillano, The relationship between diffuse auroral and plasma sheet electron distributions near local midnight, submitted to J. Geophys. Res., 1987.

Sharber, J. R., The continuous (diffuse) aurora and auroral-e ionization, Proceedings of the 1981 Conference on the Physics of Space Plasmas, edited by T. S. Chang, B.Coppi, and J. R. Jasperse, 115-140, Scientific Publishers, Cambridge, Massachusetts, 1981.

Shaw, R. R., and D. A. Gurnett, Electrostatic noise bands associated with the electron gyrofrequency and plasma frequency in the outer magnetosphere, J. Geophys. Res., 80, 4259-4271, 1975.

Swift, D. W., Mechanisms for auroral precipitation: a review, Rev. Geophys. Space Phys., 19, 185-211, 1981.

Tsurutani, B. T., and E. J. Smith, Two types of magnetospheric ELF chorus and their substorm dependencies, J. Geophys. Res., 82, 5112-5127, 1977.

Tsurutani, B. T., E. J. Smith, H. I. West, Jr., and R. M. Buck, Chorus, energetic electrons, and magnetospheric substorms, Wave Instabilities in Space Plasmas, edited by P.J. Palmadesso and K. Papadopoulous, 51-62, D. Reidel, Dordrecht, Holland, 1979.

Winningham, J. D., C. D. Anger, G. G. Shepherd, E. J. Weber, and R. A. Wagner, A case study of the aurora, high-latitude ionosphere, and particle precipitation during near-steady state conditions, J. Geophys. Res., 83, 5717-5731, 1978.

LABORATORY OPERATIONS

The Aerospace Corporation functions as an "architect-engineer" for national security projects, specializing in advanced military space systems. Providing research support, the corporation's Laboratory Operations conducts experimental and theoretical investigations that focus on the application of scientific and technical advances to such systems. Vital to the success of these investigations is the technical staff's wide-ranging expertise and its ability to stay current with new developments. This expertise is enhanced by a research program aimed at dealing with the many problems associated with rapidly evolving space systems. Contributing their capabilities to the research effort are these individual laboratories:

Aerophysics Laboratory: Launch vehicle and reentry fluid mechanics, heat transfer and flight dynamics; chemical and electric propulsion, propellant chemistry, chemical dynamics, environmental chemistry, trace detection; spacecraft structural mechanics, contamination, thermal and structural control; high temperature thermomechanics, gas kinetics and radiation; cw and pulsed chemical and excimer laser development, including chemical kinetics, spectroscopy, optical resonators, beam control, atmospheric propagation, laser effects and countermeasures.

Chemistry and Physics Laboratory: Atmospheric chemical reactions, atmospheric optics, light scattering, state-specific chemical reactions and radiative signatures of missile plumes, sensor out-of-field-of-view rejection, applied laser spectroscopy, laser chemistry, laser optoelectronics, solar cell physics, battery electrochemistry, space vacuum and radiation effects on materials, lubrication and surface phenomena, thermionic emission, photosensitive materials and detectors, atomic frequency standards, and environmental chemistry.

Electronics Research Laboratory: Microelectronics, solid-state device physics, compound semiconductors, radiation hardening; electro-optics, quantum electronics, solid-state lasers, optical propagation and communications; microwave semiconductor devices, microwave/millimeter wave measurements, diagnostics and radiometry, microwave/millimeter wave thermionic devices; atomic time and frequency standards; antennas, rf systems, electromagnetic propagation phenomena, space communication systems.

Materials Sciences Laboratory: Development of new materials: metals, alloys, ceramics, polymers and their composites, and new forms of carbon; nondestructive evaluation, component failure analysis and reliability; fracture mechanics and stress corrosion; analysis and evaluation of materials at cryogenic and elevated temperatures as well as in space and enemy-induced environments.

Space Sciences Laboratory: Magnetospheric, auroral and cosmic ray physics, wave-particle interactions, magnetospheric plasma waves; atmospheric and ionospheric physics, density and composition of the upper atmosphere, remote sensing using atmospheric radiation; solar physics, infrared astronomy, infrared signature analysis; effects of solar activity, magnetic storms and nuclear explosions on the earth's atmosphere, ionosphere and magnetosphere; effects of electromagnetic and particulate radiations on space systems; space instrumentation.